Inorganic Chemistry

Article

pubs.acs.org/IC

Influence of Halogen Bonding Interaction on Supramolecular Assembly of Coordination Compounds; Head-to-Tail N···X Synthon Repetitivity

Hamid Reza Khavasi* and Alireza Azhdari Tehrani

Faculty of Chemistry, Shahid Beheshti University, General Campus, Evin, Tehran 1983963113, Iran

Supporting Information

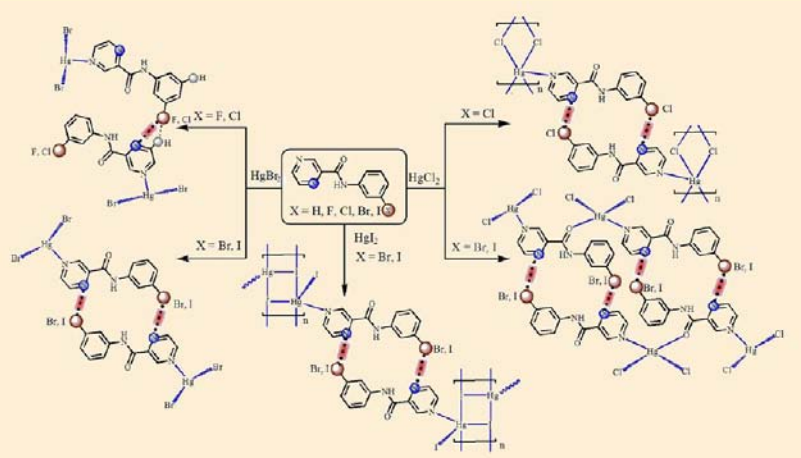

ABSTRACT: In this study, *N*-(3-halophenyl)-2-pyrazinecarboxamide ligands, $L^{3\text{-F}}$, $L^{3\text{-Cl}}$, $L^{3\text{-Br}}$, and $L^{3\text{-I}}$, carrying a different halogen atom on the phenyl *meta*-position and *N*-phenyl-2-pyrazinecarboxamide ligand, L^{H}, have been employed for the synthesis of 12 mercury(II) complexes, $[HgCl_2(L^{H})]_n$, **1**, $[HgCl_2(L^{3\text{-Cl}})]_n$, **2**, $[Hg_2Cl_4(L^{3\text{-Br}})_2]$, **3**, $[Hg_2Cl_4(L^{3\text{-I}})_2]$, **4**, $[Hg_2Br_4(L^{H})_2]$, **5**, $[HgBr_2(L^{3\text{-F}})]$, **6**, $[HgBr_2(L^{3\text{-Cl}})]$, **7**, $[HgBr_2(L^{3\text{-Br}})]$, **8**, $[HgBr_2(L^{3\text{-I}})]$, **9**, $[Hg_2I_4(L^{H})_2]$, **10**, $[HgI_2(L^{3\text{-Br}})]$, **11**, and $[HgI_2(L^{3\text{-I}})]_n$, **12**. Interestingly, structural analysis clearly shows that, by the replacing of coordinated anions from chloride with bromide and iodide in each series containing the same ligand, the coordination geometry and structural motif of the resulting compounds have been dramatically affected. One of the common features in the crystal structures of these complexes is that there is a strong tendency to form halogen bonding synthons between adjacent halophenyl and pyrazine rings. The influence of these halogen bonding interactions on the supramolecular assemblies has been discussed with the help of geometrical analysis and theoretical calculations. The X···N halogen bonding distances are 2.5−9.4% shorter than the sum of the van der Waals radii of nitrogen and halogen atoms. Theoretical methods also show the halogen bonding energies within a range of −27.86 to −46.15 kJ·mol^{-1}. In all complexes synthesized here, the pyrazine ring is coordinated to the mercury(II) ion through the N atom *syn* to the carbonyl. Therefore, the second common feature of the crystal structures for complexes studied here is the selectivity of the metal ion coordination site. The halogen bond synthon repetitivity across these compounds and selectivity in the mercury(II) ion coordination site further point to application in the coordination crystal engineering research field.

INTRODUCTION

Structural assemblies in coordination compounds rely on a range of directional and nondirectional intermolecular interactions to hold the components together. The most extensively exploited of these interactions is highly directional hydrogen bonding.[1] The influence of $\pi\cdots\pi$, cation$\cdots\pi$, anion$\cdots\pi$, lone-pair$\cdots\pi$, and metal$\cdots\pi$ interactions is also well accepted among supramolecular coordination chemists.[2] Another interaction that has more recently become of interest as a construction tool in the field of crystal engineering is directional attractive halogen bonding interaction (hereafter referred to as XB). The XB, denoted in the general form D···X−Y (Y = C, N, halogen, etc.), refers to any noncovalent interaction involving a halogen as the acceptor of electron density, a Lewis acid, and an electron-donating atom, D, as a Lewis base.[3] Various types of XB, including R-X···Nu, X_2···Nu, R-X1···X2-R, R-X1···X2-M, and R-X1···X2$^-$, where Nu is a nucleophile, R-Xi is a haloalkyl group, X_2 is a dihalogen molecule, Xi$^-$ is a halide anion, and M is a metal, have been studied in detail.[4] Although the role of XB in metal-containing crystal structures and analogies and differences with respect to hydrogen bonds have been reviewed by Brammer[5] and

Received: September 28, 2012
Published: February 26, 2013

   dx.doi.org/10.1021/ic3021113 | Inorg. Chem. 2013, 52, 2891−2905

Bertani and co-workers,[6] compared to organic systems, to our knowledge, far less attention has been paid to *systematic* studies that examine the effect of halogen bonding on the supramolecular aggregation of coordination complexes. To make progress in controlling specific interactions in the solid state of coordination compounds, it is desirable to synthesize a series of coordination compounds of predetermined chemical structure, allowing for a comparison between assemblies with specific and controllable changes to their molecular structure.

Recently, the possibility of using C═O···X (X = Cl, Br, I) halogen bonds for directed assembly in copper(II) coordination compounds containing *β*-diketonate moieties bearing chloro, bromo, and iodo substituents has been systematically studied by Aakeröy and co-workers.[7] In 2008, competition between coordination network formation and halogen bond network formation using copper(II) iodobenzoate units was reported by Brammer and co-workers.[8]

On the other hand, with the exploration of how weak interactions work individually or cooperatively in the supramolecular structure, the identification of reproducible synthons in the supramolecular structures is an important line of research.[9] In this regard, even failed attempts at supramolecular assembly can offer some insight into discovering how intermolecular interactions can be ranked in terms of structural effectiveness. Assembly of discrete copper(II) and cobalt(II) coordination compounds into 1D linear chains using halogen bond interactions has been investigated by Aakeröy, and the results showed that attempts at creating desired architectures had failed.[10] In Ward and co-worker's paper, the repetitivity of C−I···NC(Ru) halogen bonds in $[Ru(bipy)(CN)_4]^{2-}$ salts containing iodinated cations has been shown, while the analogous brominated cations do not exhibit halogen bond interactions.[11]

During our research effort on *π*−*π* stacking,[12a] C−H···*π*[12b] interaction, and ligand substituent effect[12c] in the crystal packing of mercury coordination compounds containing pyrazine carboxamide ligands, that the authors are developing, the effect of halogen bonding on the three-dimensional supramolecular architecture of coordination compounds has herein been reported. In this Article, a series of *N*-(3-halophenyl)-2-pyrazinecarboxamide ligands, $L^{3\text{-F}}$, $L^{3\text{-Cl}}$, $L^{3\text{-Br}}$, and $L^{3\text{-I}}$, and *N*-phenyl-2-pyrazinecarboxamide ligand, L^{H} (Scheme 1), carrying a different halogen atom in the phenyl *meta*-position, have been employed for the synthesis of mercury(II) complexes in order to get insights into the effect of halogen bonding interactions on the structural assembly of the complexes. Because of the freedom of C−C and C−N single bond rotations in these ligands, the pyrazine and halophenyl rings can be freely twisted to meet the requirements of the coordination geometries of metal atoms and intermolecular interactions in the assembly process. Twelve Hg(II) complexes of these ligands, $[HgCl_2(L^{H})]_n$, **1**, $[HgCl_2(L^{3\text{-Cl}})]_n$, **2**, $[Hg_2Cl_4(L^{3\text{-Br}})_2]$, **3**, $[Hg_2Cl_4(L^{3\text{-I}})_2]$, **4**, $[Hg_2Br_4(L^{H})_2]$, **5**, $[HgBr_2(L^{3\text{-F}})]$, **6**, $[HgBr_2(L^{3\text{-Cl}})]$, **7**, $[HgBr_2(L^{3\text{-Br}})]$, **8**, $[HgBr_2(L^{3\text{-I}})]$, **9**, $[Hg_2I_4(L^{H})_2]$, **10**, $[HgI_2(L^{3\text{-Br}})]$, **11**, and $[HgI_2(L^{3\text{-I}})]_n$, **12**, have been prepared by the reaction of equimolar quantities of mercury(II) halides (chloride, bromide, and iodide) in a methanol solution (Scheme 1). The structural details show that the presence of Cl, Br, and I atoms in the *meta*-position of the *N*-phenyl ring significantly influences the structural assembly of the resulting mercury(II) complexes and the ligands are pointed toward the adjacent molecules to generate simple or head-to-tail N···X (X = Cl, Br, I) halogen bond synthons.

Scheme 1. Synthetic Route of 1−12 and Presence of Halogen Bond Synthons (Red Band)

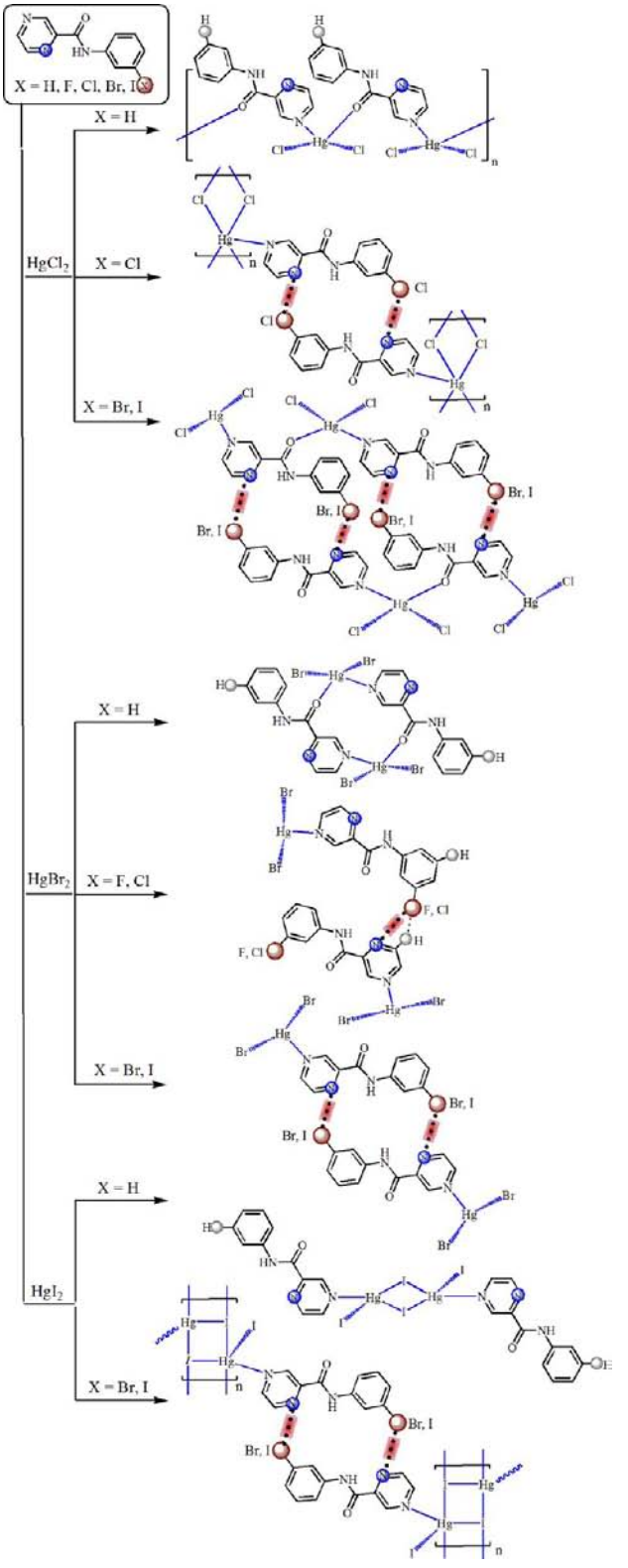

RESULTS AND DISCUSSION

Synthesis. The ligands L^{H}, $L^{3\text{-F}}$, $L^{3\text{-Cl}}$, $L^{3\text{-Br}}$, and $L^{3\text{-I}}$ were prepared by simply mixing the same equivalents of *meta*-haloaniline or aniline and pyrazinecarboxylic acid in pyridine in the presence of triphenyl phosphite.[13] The reaction of equimolar

dx.doi.org/10.1021/ic3021113 | Inorg. Chem. 2013, 52, 2891−2905

Table 1. Structural Data and Refinement Parameters for Compounds 1−12

	1	2	3	4	5	6
formula	$C_{11}H_9Cl_2HgN_3O$	$C_{11}H_8Cl_3HgN_3O$	$C_{22}H_{16}Br_2Cl_4Hg_2N_6O_2$	$C_{22}H_{16}Cl_4Hg_2I_2N_6O_2$	$C_{22}H_{18}Br_4Hg_2N_6O_2$	$C_{11}H_8Br_2FHgN_3O$
fw	470.70	505.14	1099.18	1193.18	1119.20	577.59
cryst syst	monoclinic	triclinic	monoclinic	monoclinic	monoclinic	orthorhombic
space group	$P2_1/c$	$P\bar{1}$	$P2_1/c$	$P2_1/c$	$P2_1/n$	$Pbca$
a (Å)	7.1019(11)	3.9330(8)	16.4086(2)	16.5955(12)	7.2762(10)	6.7945(4)
b (Å)	11.2071(19)	12.012(2)	13.2074(2)	13.4945(7)	15.4995(14)	12.5409(12)
c (Å)	16.435(2)	15.803(3)	13.1793(2)	13.4342(9)	12.0093(16)	33.507(2)
α (deg)	90	109.56(3)	90	90	90	90
β (deg)	91.144(12)	96.68(3)	104.4990(10)	104.954(6)	92.121(11)	90
γ (deg)	90	98.47(3)	90	90	90	90
V (Å^3)	1307.8(3)	684.8(2)	2765.19(7)	2906.7(3)	1353.5(3)	2855.1(4)
D_{calc} (Mg·m^{-3})	2.391	2.450	2.640	2.727	2.746	2.688
Z	4	2	4	4	2	8
μ (mm^{-1})	12.167	11.816	14.402	13.076	17.266	16.385
F(000)	872	468	2016	2160	1016	2096
2θ (deg)	58.40	54.00	58.60	58.60	58.42	58.66
R (int)	0.0616	0.1097	0.0519	0.0729	0.1008	0.2859
GOF	1.12	1.08	1.04	1.12	1.20	1.38
$R_1{}^a$ ($I > 2\sigma(I)$)	0.044	0.047	0.029	0.052	0.054	0.179
$wR_2{}^b$ ($I > 2\sigma(I)$)	0.140	0.115	0.053	0.124	0.139	0.360
final electron density (e·Å^{-3})	1.86, −1.97	1.63, −1.66	1.26, −1.20	2.06, −2.22	1.77, −3.76	1.74, −1.44
CCDC No.	901972	901975	901970	912465	901971	901981

	7	8	9	10	11	12
formula	$C_{11}H_8Br_2ClHgN_3O$	$C_{11}H_8Br_3HgN_3O$	$C_{11}H_8Br_2HgIN_3O$	$C_{22}H_{18}Hg_2I_4N_6O_2$	$C_{11}H_8BrHgI_2N_3O$	$C_{11}H_8HgI_3N_3O$
fw	594.04	638.49	685.49	1307.20	732.49	779.49
cryst syst	orthorhombic	monoclinic	monoclinic	monoclinic	monoclinic	monoclinic
space group	$Cmca$	$C2/m$	$C2/m$	$C2/c$	$C2/m$	$C2/m$
a (Å)	6.6796(13)	13.3681(17)	13.681(13)	7.2849(11)	13.609(2)	13.9063(13)
b (Å)	13.257(3)	6.6595(9)	6.6901(17)	12.5265(14)	6.9070(10)	6.9034(7)
c (Å)	33.744(7)	17.1358(18)	17.162(4)	33.5265(4)	17.596(3)	17.5611(17)
β (deg)	90	103.551(9)	104.740(18)	91.415(11)	102.494(12)	103.402(7)
V (Å^3)	2988.1(10)	1483.0(3)	1519.0(6)	3043.7(7)	1614.8(4)	1640.0(3)
D_{calc} (Mg·m^{-3})	2.641	2.860	2.997	2.853	3.013	3.157
Z	8	4	4	4	4	4
μ (mm^{-1})	15.823	18.455	17.419	14.162	15.824	15.028
F(000)	2160	1152	1224	2320	1296	1368
2θ (deg)	58.50	58.64	58.74	58.56	58.44	58.34
R (int)	0.1265	0.1275	0.1489	0.1118	0.1049	0.0725
GOF	1.17	1.15	1.19	1.07	1.26	1.09
$R_1{}^a$ ($I > 2\sigma(I)$)	0.059	0.094	0.077	0.131	0.063	0.047
$wR_2{}^b$ ($I > 2\sigma(I)$)	0.141	0.239	0.193	0.358	0.175	0.126
final electron density (e·Å^{-3})	2.27, −2.54	2.19, −2.71	3.25, −2.12	1.70, −1.31	2.12, −4.86	2.56, −2.30
CCDC No.	901978	901973	901974	901980	901979	901977

$^aR_1 = \sum||F_o| - |F_c||/\sum|F_o|$. $^bwR_2 = [\sum(w(F_o^2 - F_c^2)^2)/\sum w(F_o^2)2]^{1/2}$.

amounts of these ligands and HgX_2 (X = Cl, Br, and I) in methanol gave the corresponding complexes. Slow evaporation of the solvent resulted in air-stable block crystals of **1**, **3**−**5**, **8**, and **10**−**12**; prism crystals of **2**, **7**, and **9**; and needle crystals of **6**, after a few days. Attempts were made to form complexes with $HgCl_2$ and HgI_2 using the $L^{3\text{-F}}$ ligand and HgI_2 using the $L^{3\text{-Cl}}$ ligand. Yet unfortunately, no mercury-containing species were isolated from the reaction mixtures. Crystallographic data for compounds **1**−**12** are listed in Table 1. Selected bond distances and angles are summarized in Table 2.

Structural Analysis of $HgCl_2$ Complexes, $[HgCl_2(L^H)]_n$, 1, $[HgCl_2(L^{3\text{-Cl}})]_n$, 2, $[Hg_2Cl_4(L^{3\text{-Br}})_2]$, 3, and $[Hg_2Cl_4(L^{3\text{-I}})_2]$, 4. A simple reaction between $HgCl_2$ and L^H, $L^{3\text{-Cl}}$, $L^{3\text{-Br}}$, and $L^{3\text{-I}}$ in methanol afforded well-formed crystals of **1**−**4**. The asymmetric unit of **1** consists of one crystallographically independent Hg^{2+} ion, one *N*-phenyl-2-pyrazinecarboxamide, L^H, and two chloride ions. As depicted in Figure 1a, in this compound, the highly distorted tetrahedral geometry of the Hg(II) center can be better described as a seesaw structure. The Cl−Hg−Cl angle is 176.17(10)°, where the two Hg−Cl bonds form the plank (Table 2). The angle between the other two bonds (Table 2), which form the pivot, is 90.0(2)°. The Cl−Hg−Cl and N−Hg−O planes are nearly perpendicular, with a dihedral angle of 87.0(4)°. For this complex, the four-coordinate geometry index, τ_4, of 0.64 fits with a seesaw description.[14]

Compound **2** crystallizes in the $P\bar{1}$ space group. The asymmetric unit of **2** consists of one Hg^{2+} ion, two halogen anions, and one crystallographically independent ligand. As

dx.doi.org/10.1021/ic3021113 | Inorg. Chem. 2013, 52, 2891−2905

Table 2. Selected Bond Lengths (Å) and Angles (deg) around Mercury(II) for Complexes 1−12

		complex					
		1	**2**	**3**	**4**	**5**	**6**
bond distance	Hg1−X1	2.289(2)	2.3464(18)	2.3106(6)	2.295(2)	2.4147(10)	2.443(4)
	Hg1−X1		3.047(2)[a]				
	Hg1−X2	2.303(2)	2.3375(19)	2.3089(7)	2.294(2)	2.4293(0)	2.462(4)
	Hg1−X2		3.044(2)[b]				
	Hg1−O1	2.748(6)[a]				2.949(7)[c]	
	Hg1−N2	2.656(8)	2.575(5)	2.573(2)	2.599(7)	2.514(7)	2.49(3)
	Hg2−X3			2.3340(7)	2.300(2)		
	Hg2−X4			2.3088(7)	2.325(2)		
	Hg2−O1			2.815(2)	2.822(7)		
	Hg2−N5			2.516(2)	2.551(9)		
bond angle	X1−Hg1−X2	176.17(10)	173.26(6)	169.44(2)	169.81(9)	161.93(4)	163.90(15)
	X1−Hg1−X2		92.71(6)[a]				
	X1−Hg1−X1		86.82(6)[b]				
	X2−Hg1−X2		92.98(6)[b]				
	X1−Hg1−O1	92.0(1)[a]				105.8(1)	
	X2−Hg1−O1	86.6(1)[a]				82.8(1)	
	X1−Hg1−N2	93.18(18)	93.01(15)	94.30(5)	94.34(17)	101.3(2)	98.2(7)
	X2−Hg1−N2	90.40(17)	93.73(14)	95.36(5)	95.12(17)	95.8(2)	97.9(7)
	X1−Hg1−N2		91.5(5)[a]				
	X2−Hg1−N2		93.7(1)[b]				
	N1−Hg1−O1	90.0(2)[a]				79.4(2)[c]	
	Hg1−O1═C5	125.4(5)[a]				114.8(5)[c]	
	X3−Hg2−X4			166.36(3)	166.00(9)		
	X3−Hg2-N5			93.57(6)	99.32(17)		
	X3−Hg2−O1			98.53(5)	89.4(1)		
	X4−Hg2−N5			99.15(6)	93.77(17)		
	X4−Hg2−O1			88.49(5)	97.3(1)		
	N5−Hg2−O1			80.48(7)	82.34(16)		
	Hg2−O1═C5			106.8(2)	109.0(5)		

		complex					
		7	**8**	**9**	**10**	**11**	**12**
bond distance	Hg1−X1	2.4639(12)	2.459(2)	2.4569(18)	2.622(2)	2.6381(10)	2.6394(8)
	Hg1−X1				3.512(3)[d]	3.4957(5)[e]	3.5182(4)[f]
	Hg1-X2	2.4287(14)	2.424(2)	2.420(2)	2.602(2)	2.5950(11)	25953(8)
	Hg1−N2	2.469(10)	2.480(13)	2.449(13)	2.54(3)	2.474(10)	2.484(7)
bond angle	X1−Hg1−X2	161.05(5)	160.26(9)	159.07(8)	163.17(10)	156.92(4)	155.95(3)
	X1−Hg1−X2					93.63(3)[e]	94.46(2)[f]
	X1−Hg1−X1				92.61(8)[d]	89.84(3)[e]	90.06(2)[f]
	X1−Hg1−N2	98.3(3)	98.2(4)	98.8(3)	98.4(7)	102.0(2)	102.3(2)
	X2−Hg1−N2	100.6(2)	101.6(4)	102.1(3)	97.6(7)	101.0(2)	101.8(2)
	X1−Hg1-N2				94.24(8)	81.3(2)[e]	79.1(2)[f]

[a]Symmetry codes: 1 + *x*, *y*, *z*. [b]Symmetry codes: −1 + *x*, *y*, *z*. [c]Symmetry codes: −*x*, 2 − *y*, 2 − *z*. [d]Symmetry codes: 1/2 − *x*, 1/2 − *y*, −*z*. [e]Symmetry codes: 3/2 − *x*, −1/2 + *y*, −*z*. [f]Symmetry codes: 1/2 − *x*, −1/2 + *y*, 1 − *z*.

depicted in Figure 1b, the coordination geometry around the metal center is a square-based pyramid (SBP) (Table 2) with a trigonality index, τ_5,[15] of 0.03. In this structure, the plane of the square-based pyramid is occupied by four halogen anions (Table 2). The apical position is occupied by a nitrogen atom from the pyrazine ring of the $L^{3\text{-Cl}}$ ligand at a normal distance of 2.575(5) Å. As it is clear from the τ_5 value and geometrical parameters around the central metal atom (Table 2), the coordination geometry around Hg(II) is almost perfect SBP.

Dinuclear isostructural compounds **3** and **4** consist of two different mercury environments. In these compounds, each asymmetric unit consists of two crystallographically independent mercury centers, four chloride ions, and two neutral $L^{3\text{-Br}}$ or $L^{3\text{-I}}$ ligands (Figure 1c,d). The Hg1 atom is located in a three coordination environment, chelating with two chloride atoms and one pyrazine nitrogen atom from the ligand $L^{3\text{-X}}$ (X = Br, I) (Table 2). The Cl−Hg−Cl angle of 169.44(2)° and 169.81(9)° for **3** and **4**, respectively, shows that the geometry around the metal center is slightly distorted T-shaped. In these compounds, the $L^{3\text{-X}}$ ligand acts as an angular bridge *via* the carbonyl oxygen and the pyrazine nitrogen atoms to link Hg1 and Hg2 ions. The coordination geometry around the Hg2 atom in compounds **3** and **4** can be described as a seesaw structure with a τ_4 index of 0.67 for both complexes, with nearly linear Cl−Hg−Cl (Table 2) forming the plank, and N−Hg−O (Table 2) for **3** and **4** forming the pivot. The dihedral angles between the Cl−Hg−Cl and N−Hg−O planes are 83.78(6)° and 84.91(7)° for **3** and **4**,

dx.doi.org/10.1021/ic3021113 | *Inorg. Chem.* 2013, 52, 2891−2905

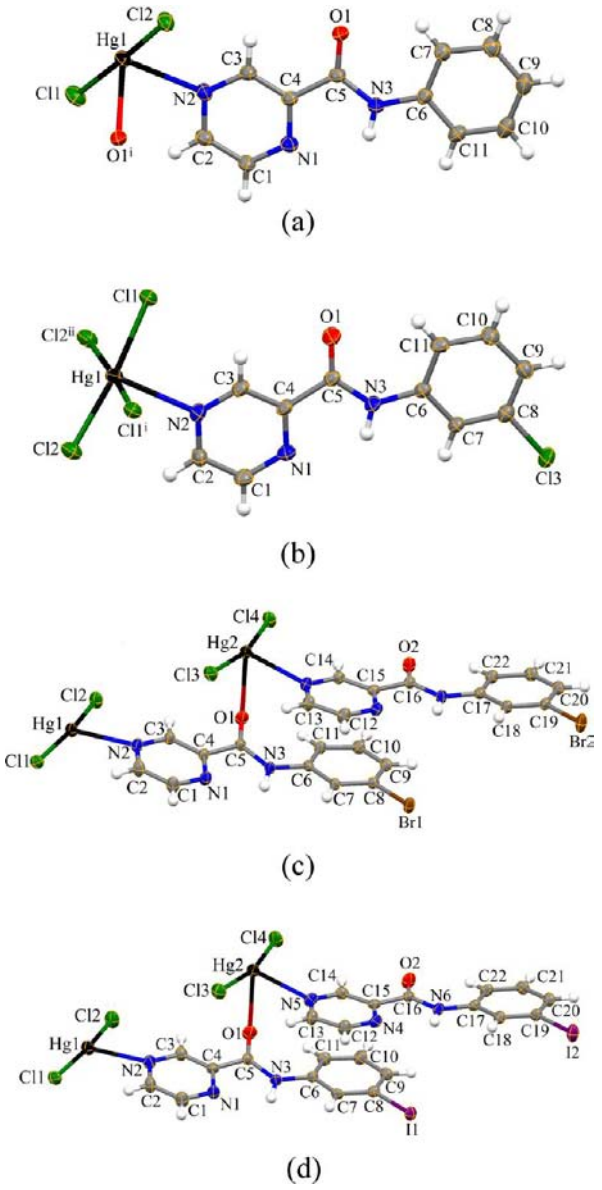

Figure 1. Portion of the structure of coordination compounds formed between $HgCl_2$ and L^H, **1** (a), $L^{3\text{-Cl}}$, **2** (b), $L^{3\text{-Br}}$, **3** (c), and $L^{3\text{-I}}$, **4** (d), showing coordination geometry around the central metal. Displacement ellipsoids are shown at 30% probability level. Symmetry codes: (a) (i) 1 + *x*, *y*, *z*; (b) (i) 1 + *x*, *y*, *z*; (ii) −1 + *x*, *y*, *z*.

respectively. We propose a simple geometry index for almost planar three-coordinate complexes, trigonal-planar index, τ_3, eq 1

$$\tau_3 = |[(\alpha + \beta + \gamma)/360] - |(\alpha - 120)/60|| \quad (1)$$

inspired by Houser's four-cooordinate τ_4 index[14] and Addison and Reedijk's five-coordinate τ_5 index.[15] In this equation, α is the largest angle in the three-coordinated complex. The values of τ_3 will range from 1.00 for a perfect trigonal-planar geometry, since $[(120 + 120 + 120)/360] - [(120 - 120)/60] = 1 - 0 = 1$, to zero for a perfect T-shaped geometry, since $[(180 + 90 + 90)/360] - [(180 - 120)/60] = 1.00 - 1.00 = 0$. Therefore, this parameter can be used for almost planar three-coordinate complexes since trigonal-planar and T-shaped geometries are the extremes. Trigonal-planar index, τ_3, for Hg1 in compound **3** and **4** is 0.17 for both complexes.

In **1**, the adjacent mercury atoms are linked by C═O−Hg bonds to form a 1D linear polymeric chain spanning along the *a* axis (Figure 2a). In this compound, the phenyl ring involved in

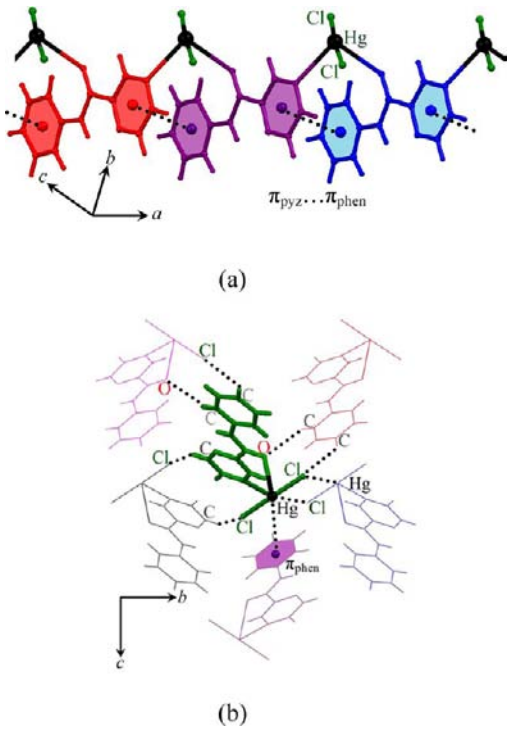

Figure 2. Representation of 1D linear polymeric chain in **1** (a), and a side view representation of **1** in the *a* direction showing the association of the adjacent molecules in the chain, through an additional head-to-tail C_{phen}−H···Cl−Hg and C═O···H−C_{phen} nonclassical hydrogen bonds and Hg···Cl contacts and Hg···π_{phen} intermolecular interactions (b). In (b), different colors show different adjacent linear chains.

the *intramolecular* $\pi-\pi$ stacking interaction with the adjecent pyrazine rings is arranged in such a way that the angle between the plane (containing C−CO−N fragment) normal and the O−Hg vector (for geometrical definition, see ref 12a) reaches about 36.81(6)°. In $\pi_{phen}\cdots\pi_{pyz}$ interactions, the centroid−centroid distance is 3.569(5) Å. Such $\pi-\pi$ interaction effects on the *primary* structure directing the coordination geometry around Hg(II), which contain similar ligands to those discussed in this paper, have previously been reported in detail by some of us.[12a] As shown in Figure 2b, these 1D linear chains are further linked to each other from one side by head-to-tail dimeric C_{phen}−H···Hg−Cl and C_{phen}−H···O═C nonclassical hydrogen bonds (Table S1, Supporting Information), and from the other side by head-to-tail Hg···Cl contacts and Hg···π_{phen} intermolecular interactions (Table 3). Coordination geometry and intermolecular interactions of compound **1** are illustrated in Scheme 2.

Within the asymmetric unit of **2**, each mercury coordinates to the nitrogen donor atom of the pyrazine ring, the N atom *syn* to the carbonyl, of the $L^{3\text{-Cl}}$ ligand, while each chloride atom in the basal plane bridges two adjacent metal centers to generate a 1D double-chain motif in the *a* direction (Figure 3a). The planar organic ligands stack along both sides of the HgCl skeleton, and the distance between their mean planes is 3.933(1) Å (Figure 3a). These 1D chains are further linked to adjacent ones by Hg···Cl contacts to generate a double chain in the *a* direction (Table 3). The resulting double chains are further linked to adjacent chains from one side by head-to-tail dimeric C_{phen}−

dx.doi.org/10.1021/ic3021113 | *Inorg. Chem.* 2013, 52, 2891−2905

Table 3. Hg···X, Hg···π, Amide···π, and π···π Distances for Compounds 1−10

complex	D−H···A	d(D···A) (Å)	symmetry
1	Hg1···Cl2	3.203(2)	$1-x, 2-y, -z$
	Hg1···π_{phen}	3.548(2)	$1+x, 3/2-y, 1/2+z$
2	Hg1···Cl1	3.198(2)	$2-x, 2-y, 1-z$
3	Hg1···Cl2	3.288(1)	$-x, 1-y, -z$
	Hg2···Cl4	3.247(1)	$-x, 1-y, -z$
	π_{phen}···π_{pyz}	3.449(4)	
	Hg1···π_{phen}	3.452(1)	$1-x, y, z$
4	Hg1···Cl3	3.324(3)	$1-x, 1-y, 1-z$
	Hg2···Cl2	3.324(3)	$1-x, 1-y, 1-z$
	π_{phen}···π_{pyz}	3.516(6)	
	Hg1···π_{phen}	3.517(4)	$x, y, -1+z$
5	π_{phen}···π_{phen}	3.847(7)	$1/2-x, 1/2+y, 5/2-z$
6	Hg1···Br2	3.378(4)	$1/2+x, 1/2-y, 2-z$
	Hg1···Br2	3.454(4)	$-1/2+x, 1/2-y, 2-z$
	amide···π_{phen}	3.475(5)	$1/2+x, y, 5/2-z$
7	Hg1···Br1	3.401(1)	$-1/2+x, 1/2-y, -z$
	amide···π_{phen}	3.373(1)	$1/2-x, y, 1/2-z$
8	Hg1···Br1	3.411(1)	$1/2-x, -1/2+y, 1-z$
	amide···π_{phen}	3.363(1)	$1/2-x, -1/2+y, 2-z$
9	Hg1···Br1	3.443(1)	$1/2-x, -1/2+y, -z$
	amide···π_{phen}	3.390(1)	$1/2-x, -1/2+y, 1-z$
10	π_{phen}···π_{pyz}	3.661(8)	$-x, y, 1/2-z$

H···O=C and C_{pyz}−H···Cl−Hg nonclassical hydrogen bonds (Figure 3b; Table S1, Supporting Information). The coordination geometry and the intermolecular interactions of compound **2** are illustrated in Scheme 2.

In isostructural **3** and **4**, the two independent dinuclear moieties are closely packed through head-to-tail Hg···Cl contacts (Table 3) to generate dimeric units (Figure 4a). Adjacent dimeric units are further linked to each other by head-to-tail N···Br/I halogen bonds (Figure 4b). In the packing of these complexes, the overall supramolecular structure results from the linkage of neighboring units of Hg···π_{phen}, C_{phen}−H···O=C, and C_{phen}−H···Cl−Hg with nonclassical hydrogen bonds (Figure 4c). Coordination geometries and intermolecular interactions of compounds **3** and **4** are illustrated in Scheme 2.

Structural Analysis of $HgBr_2$ Complexes, $[Hg_2Br_4(L^H)_2]$, 5, $[HgBr_2(L^{3\text{-}F})]$, 6, $[HgBr_2(L^{3\text{-}Cl})]$, 7, $[HgBr_2(L^{3\text{-}Br})]$, 8, $[HgBr_2(L^{3\text{-}I})]$, 9. The reaction of 1 equiv of $HgBr_2$ with 1 equiv of L^H in methanol produces a dinuclear mercury complex, **5**, with a 12-membered ring (Figure 5a). This compound displays $2/m$ point symmetry in the solid state, making half of the molecules crystallographically unique. Metal is in a seesaw geometry, with a four-coordinate geometry index, τ_4, of 0.64, coordinated by two Br atoms (Table 2) at the plank and one pyrazine nitrogen atom of the L^H ligand and one carbonyl oxygen atom of the second L^H ligand (Table 2), which form the pivot. The recent L^H ligand acts as an angular bridge *via* carbonyl oxygen and pyrazine nitrogen

Scheme 2. Representation of Coordination Geometry and Intermolecular Interactions of Compounds 1−12

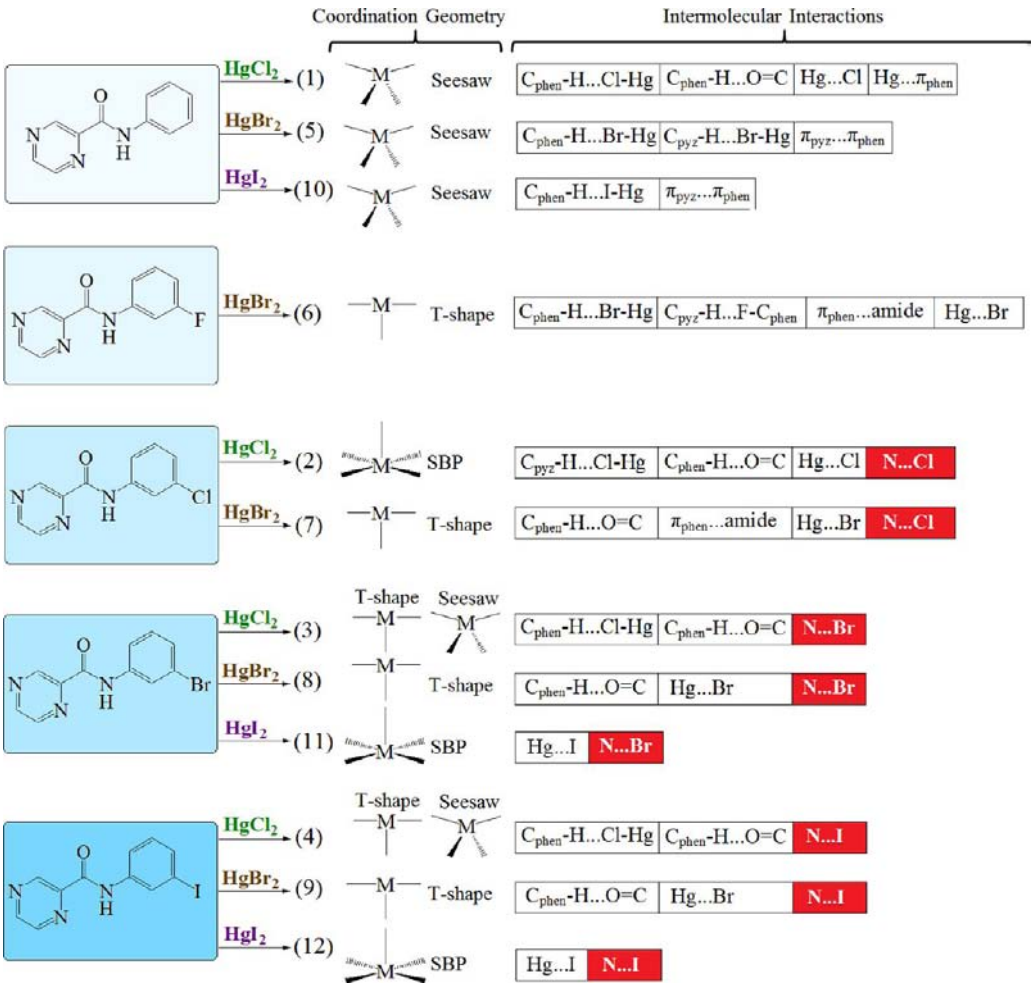

dx.doi.org/10.1021/ic3021113 | Inorg. Chem. 2013, 52, 2891−2905

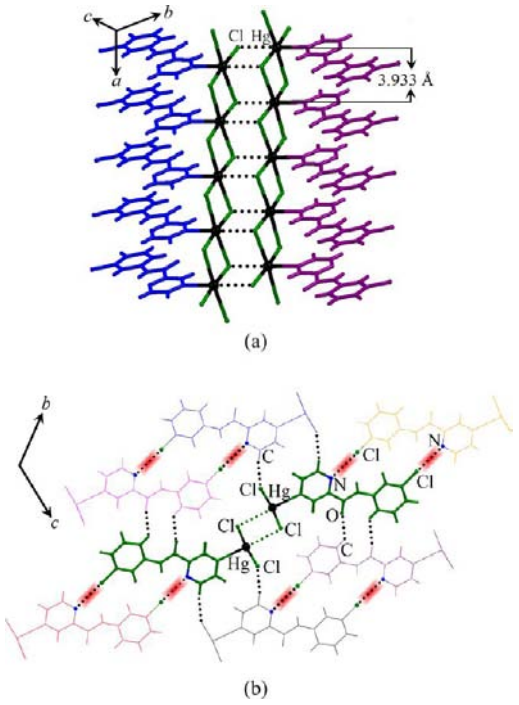

Figure 3. Representation of 1D double chain (a), and a side view representation of **2** (b), showing the association of the adjacent molecules in the chains, through head-to-tail C_{phen}–H···O=C and C_{pyz}–H···Cl–Hg nonclassical hydrogen bonds and head-to-tail N···Cl halogen bonds. Different colors show different adjacent linear chains. Halogen bonds are shown in red (b).

atoms to link Hg1 and Hg1^{i} (symmetry code: (i) $x, 2-y, 2-z$) ions. The Br–Hg–Br and N–Hg–O planes are nearly perpendicular, with a dihedral angle of 80.17(9)°.

The coordination geometries around the Hg atom in **6**–**9** are similar and made up of discrete neutral $HgBr_2L^{3\text{-}X}$ units. Figure 5b–e depicts the representative molecular structure showing the arrangement about the Hg(II) center for **6**–**9**, and selected bond distances and angles are listed in Table 2. The Hg atom lies in a T-shaped structure defined by two bromide atoms and one the pyrazine nitrogen atom of the $L^{3\text{-}X}$ ligand (Table 2). Trigonal-planar indexes, τ_3, for these compounds are 0.27, 0.32, 0.33, and 0.35, respectively (Table 4). The angle between the Br–Hg–Br plane and the pyrazine ring for **6** is 6.87(9)° and for **7**–**9** is almost 0.00°.

In **5**, the structure is stabilized by an ordered network of intermolecular $\pi\cdots\pi$ interactions that exist between the pyrazine and phenyl rings (Figure 6, Table 3). In these $\pi_{phen}\cdots\pi_{pyz}$ interactions, the centroid–centroid distance is 3.847(5) Å. As shown in Figure 6, these $\pi\cdots\pi$ interactions cooperate with C_{phen}–H···Br–Hg and C_{pyz}–H···Br–Hg to further link to each other from one side by head-to-tail dimeric Hg–Cl···H–C_{phen} nonclassical hydrogen bonds (Table S1, Supporting Information). The coordination geometry and intermolecular interactions of compound **4** are illustrated in Scheme 2.

In compounds **6**–**9**, discrete units are linked to adjacent ones by Hg···Br contacts to generate a double-stranded stair motif (Figures 7a, 8a, and 9a). In these compounds, the Hg···Br contacts of 3.378(4) and 3.454(4) Å for **6** and 3.401(1), 3.411(1), and 3.443(1) Å for **7**–**9**, respectively (Table 3), are comparable to those previously reported (3.385(1) Å) by Wu et al.[16a] The resulting double chains are further linked to adjacent chains by $\pi_{phen}\cdots$–NHCO– interactions (Figures 7a and 8a and Table 3). In **6**, these chains are further linked to adjacent chains by C_{phen}–H···Br–Hg and C_{pyz}–H···F–C intermolecular interactions (Table S1, Supporting Information), while in **7**–**9**, cooperation of N_{pyz}···Cl/Br/I halogen bonds and C_{phen}–H···O=C nonclassical hydrogen bonds are main factors in the generation of supramolecular assemblies (Figures 7b, 8b, and 9b). It is notable that compounds **8** and **9** have isostructural coordination geometries, and intermolecular interactions of compounds **6**–**9** are illustrated in Scheme 2.

Structural Analysis of HgI_2 Complexes, $[Hg_2I_4(L^H)_2]$, 10, $[HgI_2(L^{3\text{-}Br})]_n$, 11, and $[HgI_2(L^{3\text{-}I})]_n$, 12. In compound **10**, the metal center has the same seesaw geometry observed in compounds **1** and **5**, with two iodide atoms as the plank, and one iodide and one pyrazine nitrogen atom in the pivot position (Table 2). For this complex, the four-coordinate geometry index, τ_4, is 0.70. In this compound, each discrete molecular unit consists of a centrosymmetric dinuclear iodo-bridge Hg_2I_2 fragment. This bridged Hg_2I_2 forms a unsymmetric tetra-atomic rhombohedral plane (Figure 10a).

In 1D structures of **11** and **12**, each asymmetric unit consists of one crystallographically independent Hg center, two iodide ions, and one neutral $L^{3\text{-}Br}$ or $L^{3\text{-}I}$ ligand. In both structures, the coordination geometry around the Hg center is square-based pyramid (SBP) (Figure 10b,c), respectively, with a trigonality index, τ_5, of 0.09 and 0.03, respectively. In both structures of **11** and **12**, the plane of square-based pyramid is occupied by iodide anions (Table 2). The apical position in both structures is occupied by a nitrogen atom from the pyrazine ring of the L ligand at a normal distance of 2.474(10) and 2.484(7) Å for **11** and **12**, respectively. As it is clear from the τ_5 values and geometrical parameters around the central metal atoms (Table 2), Hg has a slightly distorted SBP environment in both compouds.

In **10**, the dinuclear units are further linked to adjacent ones from one side by C_{phen}–H···I–Hg nonclassical hydrogen bonds (Figure 11a) and from the other side by $\pi_{pyz}\cdots\pi_{phen}$ intermolecular interactions (Figure 11b and Table 3). The coordination geometry and intermolecular interactions of compound **10** are illustrated in Scheme 2.

In **11** and **12**, the arrangement of the asymmetric units defines the well-known double-stranded stair motif[16] (Figure 12a). In this stair 1D polymer, the translation axis is parallel to the *b* direction. In these compounds, the Hg–I bond distance of 3.4957(5) and 3.5182(4) Å is comparable to that previously reported (3.3773(5) Å) by Popovic et al.[16b] The I1 atom adopts a μ_3 mode to bridge three Hg atoms, while I2 is coordinated to metal centers as a terminal ligand. The iodide anion in the stair is tricoordinated with distorted T-shaped geometry (diagonal I···I = 4.3733(9) and 4.4005(6) Å for **11** and **12**, respectively). The organic ligand moieties approximately preserve their planarity and stack along both sides of the HgI skeleton (Figure 12a). These 1D chains are further linked by head-to-tail N_{pyz}···Br/I halogen bonds in the other direction (Figure 12b). Coordination geometries and intermolecular interactions of compounds **11** and **12** are illustrated in Scheme 2.

Influence of Halide Counteranion and Halogen Bonding on Coordination Geometry and Supramolecular Assembly. Progress in controlling the structural assemblies of coordination complexes in the solid state requires investigation of the families of compounds designed so that the effects of different factors on the resultant supramolecular and structural properties may be systematically delineated. In this regard, the effect of halogen bonding and the effect of different halogen

dx.doi.org/10.1021/ic3021113 | *Inorg. Chem.* 2013, 52, 2891–2905

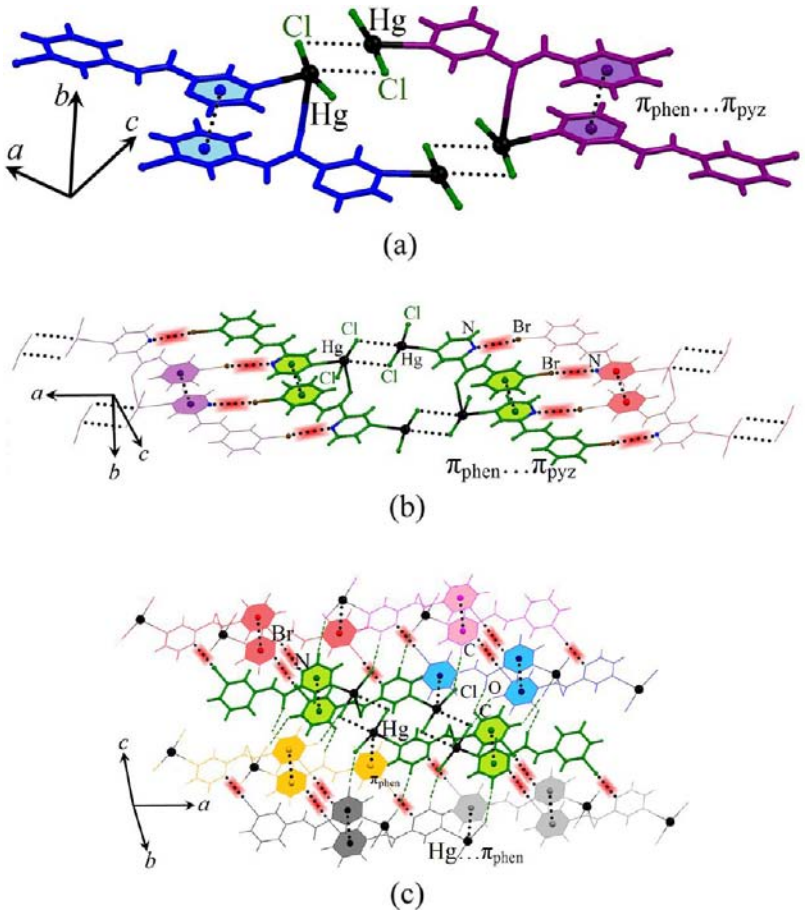

Figure 4. Side view representation of **3**, showing the generation of dimeric moieties through the Hg···Cl short contacts (a), and head-to-tail N···Br halogen bonds between adjacent dimeric units; halogen bonds are shown in red (b). A representation of part of **3** (c), showing the cooperation of head-to-tail N···Br halogen bonds, Hg···π_{phen}, C_{phen}–H···O=C, and C_{phen}–H···Cl–Hg nonclassical hydrogen bonds in generation of three-dimensional packing. Different colors show different adjacent moieties; halogen bonds are shown in red.

anions on the coordination geometry and supramolecular architecture of the 12 coordination compound of mercury(II) have been studied. Much of the difference in the structural motifs can be explained by the changing of the halogen atom on the halophenyl ring, but the role of the different halogen ions should not be neglected. Therefore, in the following discussion, first, we will focus on controlling the effect of the coordinated anion on the structural motif of the resulting coordination compounds.

Influence of Halide Anion on Coordination Geometry and Supramolecular Assembly. It is well-known that anions play an important role in the crystal engineering of self-assembled coordination polymers.[17] Some of us have recently demonstrated that cooperative noncovalent interactions can lead to the formation of one- or two-dimensional architectures under anion-directed self-assembly.[18]

Interestingly, structural analysis clearly shows that, by the replacing of coordinated anions from chloride with bromide and iodide in each series containing the same ligand, the coordination geometry and structural motif of the resulting compounds have been dramatically affected. It seems that the size of the coordinated halides would make a substantial contribution to the local mercury coordination environment and can also affect the extended structures.[17a,18,19] In compounds **1**, **5**, and **10**, where the carboxamide ligand, L^H, is similar, all complexes have the same seesaw coordination geometries (Table 4, Scheme 2). Compound **1** shows a 1D linear chain structure. The situation for compounds **5** and **10** (where the chloride anion is replaced by bromide and iodide) is quite different from that of compound **1**. The different structural motifs between **1**, **5**, and **10** are seemingly attributed to the anion size effect. Unlike the formation of the 1D linear chain in **1**, the bulkier Br and I ions in **5** and **10** are sterically hindered to form a larger aggregate. By replacing the coordinated anion from chloride to bromide and iodide, the supramolecular structure changed from 1D linear chains to dinuclear units (Table 4). Similar results were also observed for complexes **2** and **7**. For complexes containing the $L^{3\text{-Cl}}$ ligand with $HgCl_2$ and $HgBr_2$, **2** and **7**, the coordination sphere changes from SBP for **2** to T-shape for **7** (Table 4, Scheme 2). The structural motifs in these compounds are also quite different, and the 1D double chain in **2** is changed to a discrete monomer structure in **7**.

For HgX_2 adducts, while the carboxamide ligand is $L^{3\text{-Br}}$, from **3** to **8** and to **11** (where counteranions are chloride, bromide, and iodide, resepectively), the coordination sphere changes from the seesaw/T-shape (for two crystallographically independent metal ions) in **3**, to a T-shape in **8** and SBP in **11** (Table 4, Scheme 2). As listed in this table, compounds **3** and **8** show dinuclear and monuclear structures, respectievely, whereas compound **11** has a 1D ladder chain structure. In the case of **11**, although increasing the size of the anion results in the formation of a larger molecular complex, the study of Hg–I distances indicates that two of the four Hg–I bond lengths in the basal plane, connecting Hg metal

dx.doi.org/10.1021/ic3021113 | *Inorg. Chem.* 2013, 52, 2891–2905

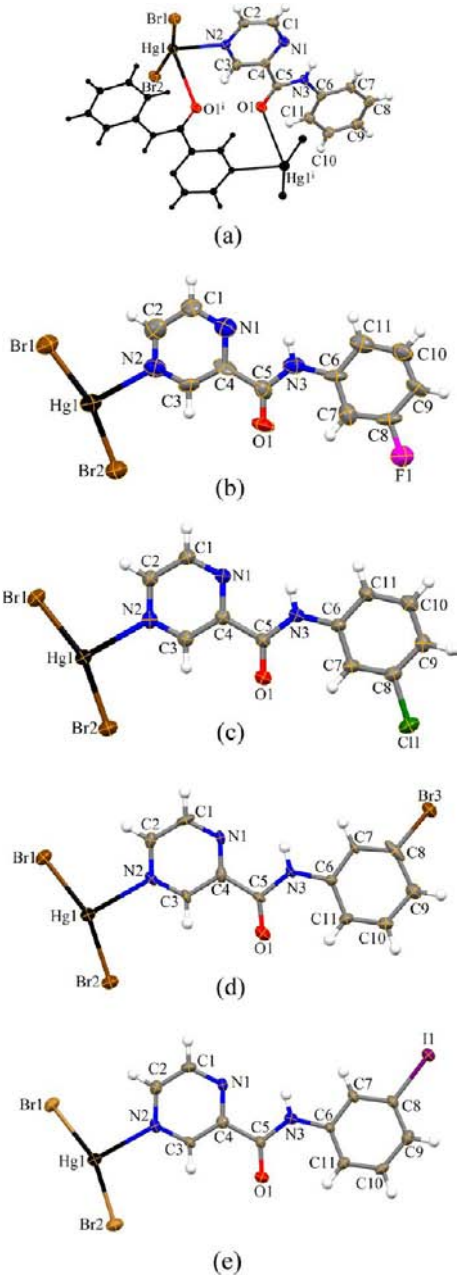

Figure 5. Structure of coordination compounds formed between $HgBr_2$ and L^H, **5** (a), $L^{3\text{-}F}$, **6** (b), $L^{3\text{-}Cl}$, **7** (c), $L^{3\text{-}Br}$, **8** (d), and $L^{3\text{-}I}$, **9** (e), showing coordination geometry around the central metal. Displacement ellipsoids are shown at 30% probability level. Symmetry codes: (i) $-x$, $2-y$, $2-z$.

centers through a Hg–I–Hg bridge, are much longer than the others, 3.496(1) Å, compared to the remaining Hg–I bond lengths, and deviate considerably from the average bond length (Table 2). It is noteworthy that a search of the Cambridge Structural Database[20] for the Hg–I distance shows that there are only 8 out of a total of 468 hits that have values longer than 3.496 Å. In the recent series, the structural analysis confirms that, as the size of the counteranion increases, the extended structures change significantly. It can be anticipated that the halide steric factor cannot be the only factor dictating the coordination environment and extended structures but certainly plays an important role in this regard.

As compounds **3** and **4**, **8** and **9**, and **11** and **12** are isostructural, for HgX_2 adducts, while the carboxamide ligand is $L^{3\text{-}I}$ (compounds **4**, **9**, and **12**), the same trend as $L^{3\text{-}Br}$ (compounds **3**, **8**, and **11**) is observed (Table 4, Scheme 2).

Influence of N···X Halogen Bonding Interaction on Supramolecular Assembly. The compounds studied here were designed to probe the influence of halogen bonding interactions on the supramolecular assembly of similar coordination compounds. Organic ligands with flexible torsions can indeed generate dissimilar conformations with different halogen bond patterns and packing modes. The common feature in the crystal structures of complexes obtained from the reaction between HgX_2 and $L^{3\text{-}Cl}$, $L^{3\text{-}Br}$ and $L^{3\text{-}I}$ ligands is the existence of a N···X halogen bond. Thus, a systematic evaluation of supramolecular synthons consisting of N···X halogen bonding interactions in a series of conformationally flexible mercury complexes containing halophenyl pyridazinamides is interesting.

In these compounds, since the halophenyl ring is flexible in rotation around the $N_{amide}-C_{phen}$ bond, this allows subtle conformational adaptation of $L^{3\text{-}X}$ to produce additional synthons *via* the rotation of the halophenyl ring. In all Hg(II) complexes reported here, the coordination of the pyrazine ring occurred through the N atom *syn* to the carbonyl and the N atom *anti* to the carbonyl is involved in classical *intramolecular* N–H···N hydrogen bonds. Because of the presence of such intramolecular hydrogen bonds, the pyrazine-CONH moiety is approximately planar, and C5=O1 and C4–N1 bonds are in the *anti* position. Therefore, the conformational variation of $L^{3\text{-}X}$ can be discussed by a dihedral angle of O1=C5–C8–X, which is listed in Table 5 for compounds **1**–**12**. As in compounds **3** and **4**, each asymmetric unit consists of two crystallographically independent $L^{3\text{-}X}$ ligands; two different values for this angle are listed in Table 5. According to the direction of the C=O and C–X bonds, the $L^{3\text{-}X}$ ligands can be arranged in *anti* and *syn* conformations (Scheme 3). In the presence of this flexibility, the halogen atom of the halophenyl ring is pointed toward the adjacent molecule to generate different synthons. Two basic halogen bond synthons (Scheme 3) were observed in the mercury complexes examined. Compound **7** adopts the *syn* conformation while the others, **2**, **3**, **4**, **8**, **9**, **11**, and **12**, adopt *anti* conformations. It is notable that these two different conformations play different roles in the formation of packing. The *syn*-conformational $L^{3\text{-}Cl}$ ligand generates a single Cl···N halogen bond in **7**, whereas in the complexes of HgX_2 with $L^{3\text{-}Br}$ and $L^{3\text{-}I}$, and also $HgCl_2$ with $L^{3\text{-}Cl}$, the *anti*-conformational ligands generate a head-to-tail halogen bond synthon (Table 5).

Table 5 provides a summary of the geometrical parameter of the halogen bonding synthons observed in **2**–**4**, **7**–**9**, **11**, and **12**. These results show that there is a strong tendency to form halogen bonding synthons between adjacent halophenyl and pyrazine rings, in order to stabilize the packing of these compounds. As it is clear from Table 5, halogen bonds show geometries consistent with a donor–acceptor binding model in which the pyrazine nitrogen atom serves as the electron donor and the halocarbon C–X bond serves as the acceptor. In complexes containing the $L^{3\text{-}Cl}$ ligand, **2** and **7**, contact distances of Cl···N were 3.190(6) and 3.217(5) Å, respectively (Table 5), indicating a 3.3% and 2.5% reduction of the sum of van der Waals radii.[21] The Br···N halogen bonding distances in compounds **3**, **8**, and **11**, complexes containing the $L^{3\text{-}Br}$ ligand, were found between 3.100(3) and 3.251(9) Å, which are 8.8–4.4% shorter than the sum of the van der Waals radii of nitrogen and bromide atoms.[21]

dx.doi.org/10.1021/ic3021113 | *Inorg. Chem.* 2013, 52, 2891–2905

Table 4. Coordination Geometries and τ_i Values of Compounds 1−12

compound	coordination geometry	τ_i	polymeric/nonpolymeric
1, $[HgCl_2(L^{H})]_n$	seesaw	$\tau_4 = 0.64$	1D linear chain
2, $[HgCl_2(L^{3\text{-}Cl})]_n$	SBP	$\tau_5 = 0.03$	1D double chain
3, $[Hg_2Cl_4(L^{3\text{-}Br})_2]$	T-shape/seesaw	$\tau_3 = 0.17/\tau_4 = 0.67$	dinuclear
4, $[Hg_2Cl_4(L^{3\text{-}I})_2]$	T-shape/seesaw	$\tau_3 = 0.17/\tau_4 = 0.67$	dinuclear
5, $[Hg_2Br_4(L^{H})_2]$	seesaw	$\tau_4 = 0.64$	cyclic dinuclear
6, $[HgBr_2(L^{3\text{-}F})]$	T-shape	$\tau_3 = 0.27$	monomer
7, $[HgBr_2(L^{3\text{-}Cl})]$	T-shape	$\tau_3 = 0.32$	monomer
8, $[HgBr_2(L^{3\text{-}Br})]$	T-shape	$\tau_3 = 0.33$	monomer
9, $[HgBr_2(L^{3\text{-}I})]$	T-shape	$\tau_3 = 0.35$	monomer
10, $[Hg_2I_4(L^{H})_2]$	seesaw	$\tau_4 = 0.70$	dinuclear
11, $[HgI_2(L^{3\text{-}Br})]_n$	SBP	$\tau_5 = 0.09$	1D ladder chain
12, $[HgI_2(L^{3\text{-}I})]_n$	SBP	$\tau_5 = 0.03$	1D ladder chain

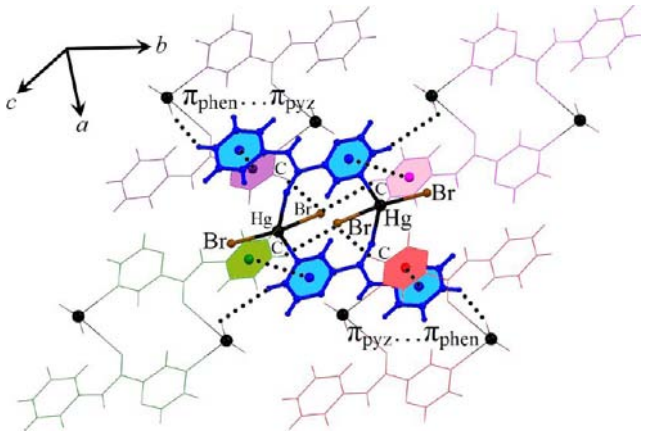

Figure 6. Side view representation of **5**, showing the cooperation of $\pi_{pyz}\cdots\pi_{phen}$ interactions and C_{phen}−H···Br−Hg and C_{pyz}−H···Br−Hg nonclassical hydrogen bonds in generation of three-dimensional packing. Different colors show different adjacent moieties.

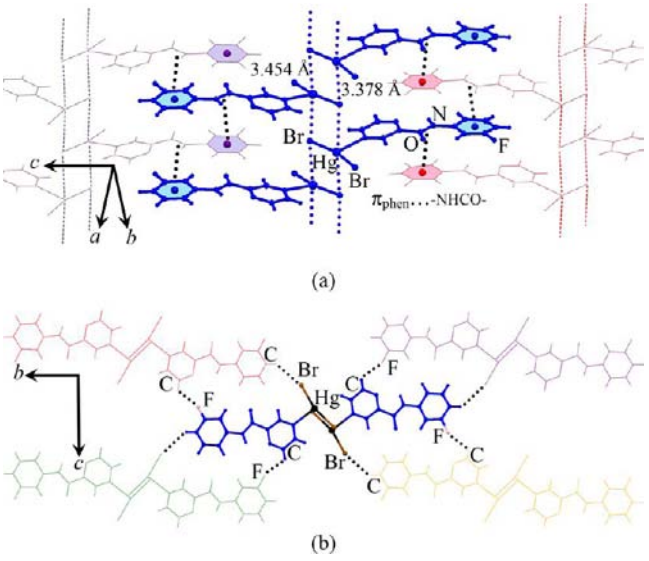

Figure 7. Side view representation of **6**, showing the generation of double-stranded stair motifs through the Hg···Br short contacts, and $\pi_{phen}\cdots$amide interactions between adjacent chains (a). A representation of part of **6** in the *a* direction (b), showing the cooperation of C_{phen}−H···Br−Hg and C_{pyz}−H···F−C intermolecular interactions in generation of three-dimensional packing. Different colors show different adjacent moieties.

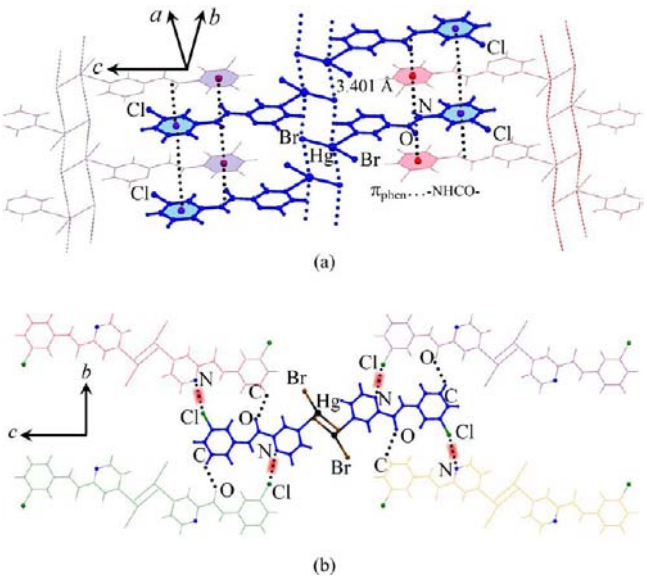

Figure 8. Side view representation of **7**, showing the generation of double-stranded stair motifs through the Hg···Br short contacts, and head-to-tail $\pi_{phen}\cdots$amide interactions between adjacent chains (a). A representation of part of **7** in the *a* direction (b), showing the cooperation of $N_{pyz}\cdots$Cl halogen bond and C_{phen}−H···O═C nonclassical hydrogen bonds in generation of three-dimensional packing. Different colors show different adjacent moieties; halogen bonds are shown in red.

Since iodide is the most polarizable atom, it would have a higher positive charge than bromide and chloride. This should also affect the intermolecular bond strength, which is indeed reflected in the observed distance between I and N (of C−I···N) (Table 5). The C−I···N intermolecular distances in compounds **4**, **9**, and **12**, containing the $L^{3\text{-}I}$ ligand, were found to be between 3.198(7) and 3.300(9) Å, which are 9.4−6.5% shorther than the sum of the van der Waals radii of nitrogen and iodide atoms.[21]

As expected,[22] Table 5 shows that the strength of the halogen bond increases from chloride to bromide and further to iodide. Besides the N···X distance, another contributing factor to halogen bond strength is the halogen bond angle C−X···N. The C−X···N angles are all close to linearity, which is consistent with the theory of electron donation into the C−X σ^* orbitals of the X-bond donor.[23]

The Cambridge Structural Database (CSD) was analyzed for halogen bonding of **2**−**4**, **7**−**9**, **11**, and **12** to determine the common range of NM−X···N interactions, where NM is a nonmetal and nonhalogen and X is Cl, Br, or I (Figure 13).[20]

dx.doi.org/10.1021/ic3021113 | *Inorg. Chem.* 2013, 52, 2891−2905

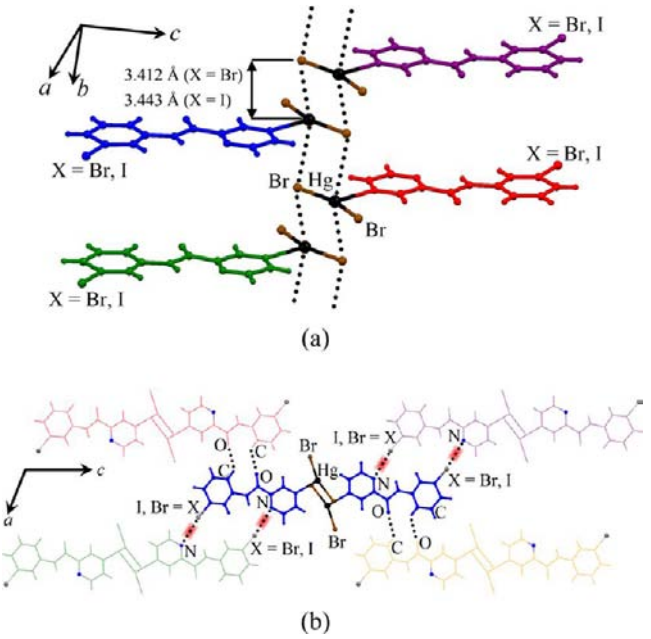

Figure 9. Side view representation of **8** and **9**, showing the generation of double-stranded stair motifs through the Hg···Br short contacts (a), and cooperation of N_{pyz}···Br/I halogen bond and C_{phen}–H···O=C nonclassical hydrogen bonds in generation of three-dimensional packing (b). Different colors show different adjacent moieties; halogen bonds are shown in red.

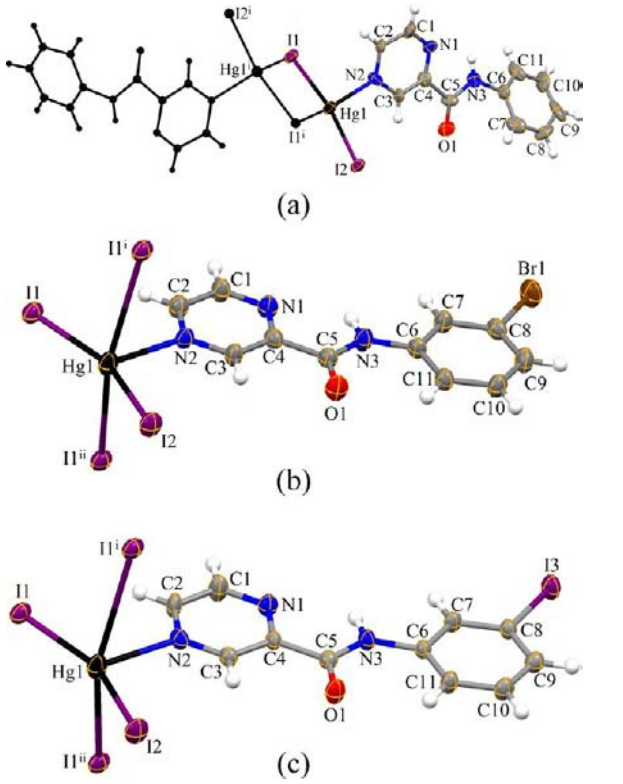

Figure 10. Portion of the structure of coordination compounds formed between HgI_2 and L^{H}, **10** (a), $L^{3\text{-}Br}$, **11** (b), and $L^{3\text{-}I}$, **12** (c), showing coordination geometry around the central metal. Displacement ellipsoids are shown at 30% probability level. Symmetry codes: (a) (i) $1/2 - x, 1/2 - y, -z$; (b) (i) $3/2 - x, -1/2 + y, -z$; (ii) $3/2 - x, 1/2 + y, -z$; (c) (i) $1/2 - x, -1/2 + y, 1 - z$; (ii) $1/2 - x, 1/2 + y, 1 - z$.

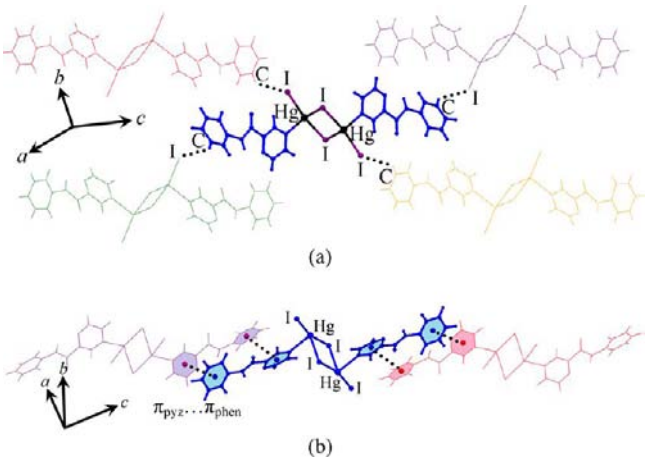

Figure 11. Side view representation of **10** showing the association *via* $C–H_{phen}$···I–Hg nonclassical hydrogen bonds (a), and π_{pyz}···π_{phen} intermolecular interactions (b), in the generation of three-dimensional packing. Different colors show different adjacent linear moieties.

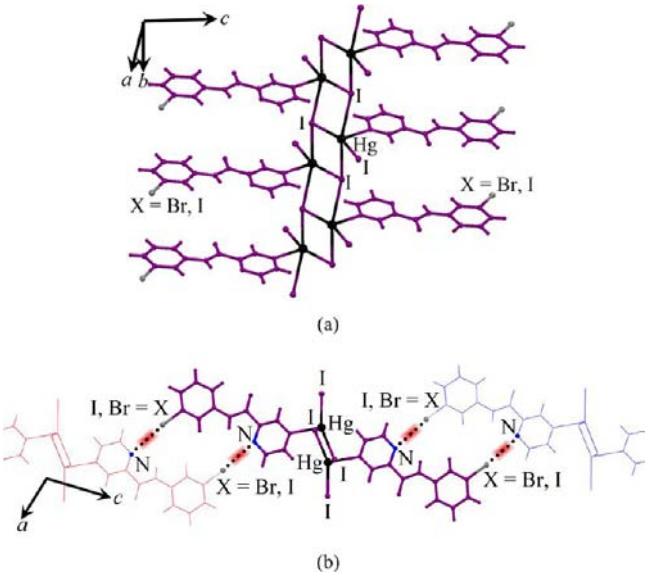

Figure 12. Side view representation of **11** and **12**, showing the generation of double-stranded stair motifs through the Hg–I bonds (a), and N_{pyz}···Br/I halogen bond in generation of three-dimensional packing (b). Different colors show different adjacent moieties; halogen bonds are shown in red.

Similar plot correlations have been reported for C–I···N halogen bonds.[24] This figure reveals that all parameters for determining these interactions are in the normal range. Therefore, it seems that the driving force for the crystal formation of these compounds is a halogen bond between the pyrazine nitrogen atom and the halogen atom on the halophenyl ring. It was thought of interest to further investigate the XB energy in these compounds by using theoretical methods. The binding energies obtained from DFT on two relative fragments (from complexes **2**–**4**, **7**–**9**, **11**, and **12**) provide us an opportunity to evaluate the complexes involving XB interactions. Calculations were performed with the experimental structures as the starting point at the LDA-ZORA-TZP level. The outcomes obtained from DFT methods are listed in Table 5. From these data, it is explicit that halogen bonding energies vary within a range of −27.86 to −46.15 kJ·mol^{-1}. In view of the directionality and

dx.doi.org/10.1021/ic3021113 | *Inorg. Chem.* 2013, 52, 2891–2905

Table 5. Halogen Bond, Conformational Parameters, and Calculated XB Binding Energies for Compounds 2−4, 7−9, 11, and 12

complex	X···N	X···N (Å)	C−X···N (deg)	reduction of the sum of the van der Waals radii (%)	symmetry code	XB synthon	$L^{3\text{-}X}$ conformation	**O1**=C5−C8−X torsion angle (deg)	calculated XB energy (kJ/mol) (LDA-Zora-TZP)
					X = Cl				
2, $[HgCl_2(L^{3\text{-}Cl})]_n$	Cl···N	3.190(6)	172.7(3)	3.3	$1-x, -y, -z$	I	*anti*	4.16(6)	−46.15
7, $[HgBr_2(L^{3\text{-}Cl})]$	Cl···N	3.217(5)	163.5(5)	2.5	$1-x, 1/2+y, 1/2-z$	II	*syn*	0.00	−27.86
					X = Br				
3, $[Hg_2Cl_4(L^{3\text{-}Br})_2]$	Br···N	3.100(3)	173.6(1)	8.8	$-x, 1-y, 1-z$	I	*anti*	6.64(5)	−39.84
		3.188(3)	170.9(1)	6.2	$-x, 1-y, 1-z$	I	*anti*	29.72(8)	
8, $[HgBr_2(L^{3\text{-}Br})]$	Br···N	3.201(17)	171.0(8)	6.1	$-x, y, 2-z$	I	*anti*	0.00	−34.06
11, $[HgI_2(L^{3\text{-}Br})]$	Br···N	3.251(9)	173.1(5)	4.4	$1-x, y, 1-z$	I	*anti*	0.00	−32.35
					X = I				
4, $[Hg_2Cl_4(L^{3\text{-}I})_2]$	I···N	3.198(7)	175.3(2)	9.4	$-x, 1-y, 2-z$	I	*anti*	6.49(8)	−44.02
		3.288(7)	170.7(2)	6.9	$-x, 1-y, 2-z$	I	*anti*	32.44(9)	
9, $[HgBr_2(L^{3\text{-}I})]$	I···N	3.248(18)	174.3(5)	8.0	$-x, y, 1-z$	I	*anti*	0.00	−41.59
12, $[HgI_2(L^{3\text{-}I})]$	I···N	3.300(9)	174.2(3)	6.5	$1-x, y, -z$	I	*anti*	0.00	−39.48

Scheme 3. Halogen Bonding Synthons Exhibited in Hg(II) Complexes

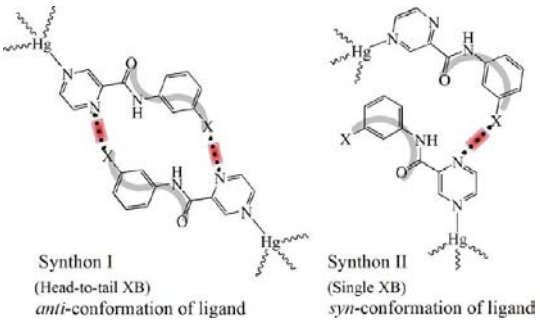

strength of the halogen bonds, the N_{pyz}···Cl/Br/I interaction can be recognized as an effective driving force to determine the alignment of molecules in supramolecular assemblies, which enables the design and development of new functional solid material.

The decomposition behavior of these compounds was also investigated in a static air atmosphere from ambient conditions to 500 °C. Stacked TG curves of compounds **2**, **3**, **4**, **7**, **8**, **9**, **11**, and **12** are given in Figure S1 (Supporting Information). The thermogravimetric analyses reveal that these compounds have identical single-step decomposition patterns.

CONCLUSION

The coordination geometry and supramolecular architecture of the 12 coordination compounds of mercury(II) halides based on $L^{3\text{-}X}$ ligands (L = *N*-(3-halophenyl)-2-pyrazinecarboxamide) carrying a different halogen atom in the phenyl *meta*-position and L^{H} (L = *N*-phenyl-2-pyrazinecarboxamide) have been studied. Structural analysis clearly shows that the size of the coordinated halides would make a substantial contribution to the local mercury coordination environment and can also affect the extended structures. In each series containing the same ligand, the bulkier Br and I ions are sterically hindered to form a larger molecule. The crystal packing of the studied compounds is determined mostly by C−H···O/X (X = F, Cl, Br, I) nonclassical hydrogen bonds and $\pi\cdots\pi$/Hg/amide and Hg···X intermolecular interactions. Since the halophenyl ring is flexible in rotation around the N_{amide}−C_{phen} bond, it allows for subtle conformational adaptation of $L^{3\text{-}X}$ (X = Cl, Br, I) to produce additional halogen bond synthons *via* the rotation of the halophenyl ring. In view of the directionality and strength of the halogen bonds, the N_{pyz}···Cl/Br/I interaction can be recognized as an effective

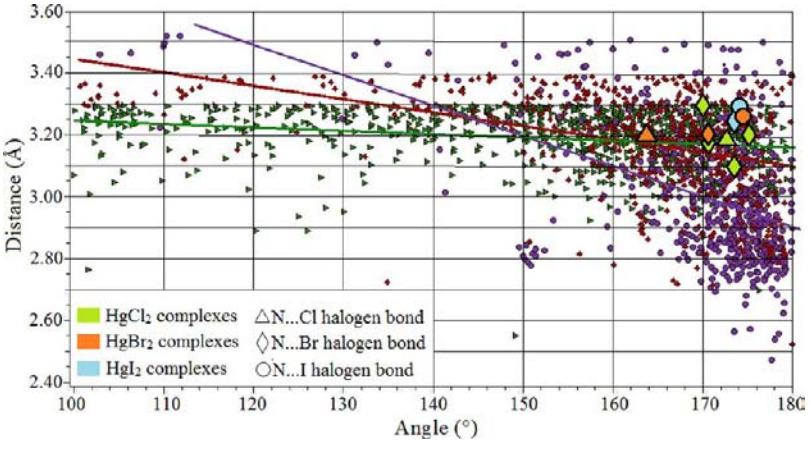

Figure 13. Scatter plot of the halogen bonding distance X···N versus the angle of NM−X···N (where NM is a nonmetal and nonhalogen). X is Cl, Br, or I shown in deep green, brown, and purple, respectively. Reported data were obtained from CSD, version 2011, filtered to include only error-free, nondisordered structures with *R*, 0.075. Correlation values: chloride, 0.243; bromide, 0.438; iodide, 0.489.

dx.doi.org/10.1021/ic3021113 | *Inorg. Chem.* 2013, 52, 2891−2905

driving force to determine the alignment of molecules in supramolecular assemblies. The N···X halogen bonding distances are 2.5−3.3, 4.4−8.8, and 6.5−9.4% shorter than the sum of the van der Waals radii of nitrogen and halogen in complexes containing $L^{3\text{-Cl}}$, $L^{3\text{-Br}}$, and $L^{3\text{-I}}$ ligands, respectively. Theoretical methods show that the halogen bonding energies within a range of −27.86 to −46.15 kJ·mol^{-1} are comparable to classical hydrogen bonding. The presence of a strong tendency to form halogen bonding synthons between adjacent halophenyl and pyrazine rings is one of the common features in the crystal structures of these complexes. Structural analysis of complexes studied here has clearly resulted in new sets of ligands that have been especially developed for selective and efficient metal coordination. Designing ligands that can provide capabilities for selective metal ion coordination is one of the important factors in controlling the architecture of self-assembled species. In all complexes synthesized here, the pyrazine ring is coordinated to the mercury(II) ion through the N atom *syn* to the carbonyl. Accordingly, the second nitrogen of the pyrazine ring, the N atom *anti* to the carbonyl, is now available to serve as a halogen bond acceptor to interact with the halogen atom. Therefore, the second common feature of the crystal structures of complexes studied here is the selectivity of the metal ion coordination site. The similarity of the halogen bond synthon across these compounds and selectivity in the mercury(II) ion coordination site further point to their application in coordination crystal engineering especially in the clever design of such special metal species and the crystal structure prediction research field.

EXPERIMENTAL SECTION

General. All chemicals were purchased from Aldrich or Merck and used without further purification. The synthesis and recrystallization of L^{H}, $L^{3\text{-F}}$, $L^{3\text{-Cl}}$, $L^{3\text{-Br}}$, and $L^{3\text{-I}}$, and mercury(II) complexes **1**−**12** were carried out in air. The ^{1}H NMR spectrum was recorded on a Bruker AC-300 MHz spectrometer at ambient temperature in CD_3OD. All chemical shifts are quoted in parts per million (ppm) relative to tetramethylsilane. Infrared spectra (4000−250 cm^{-1}) of the solid sample were taken as 1% dispersion in CsI pellets using a BOMEM-MB102 spectrometer. Elemental analysis was performed using a Heraeus CHN-O Rapid analyzer. Melting points were obtained by a Bamstead Electrothermal type 9200 melting point apparatus and corrected. All ligands were prepared according to the reported procedure.[13]

Single-Crystal Diffraction Studies. For crystals **1**−**9**, **11**, and **12**, intensity data were collected using a Bruker SMART APEX-II CCD diffractometer, equipped with a fine focus 1.75 kW sealed tube with Mo Kα radiation (λ, 0.71073 Å). The total number of images was based on the results from the program COSMO.[2Sa] Cell parameters were retrieved using APEX II software[2Sb] and refined using SAINT on all observed reflections. Data reduction was performed using the SAINT software,[2Sc] which corrects for the Lorentz and polarizing effects. Scaling and absorption corrections were applied using the SADABS[2Sd] multiscan technique, supplied by George Sheldrick. X-ray data for compound **10** were collected on a STOE IPDS-II diffractometer with graphite monochromated Mo Kα radiation (λ, 0.71073 Å). Data were collected in a series of ω scans in 1° oscillations and integrated using the Stöe X-AREA[26a] software package. A numerical absorption correction was applied using the X-RED[26b] and X-SHAPE[26c] software. All structures were solved by direct methods using SHELXS-97[27] and refined with full-matrix least-squares on F^2 using the SHELXL-97[27] program package. All non-hydrogen atoms were refined anisotropically. Hydrogen atoms were added at ideal positions and constrained to ride on their parent atoms, with $U_{iso}(H) = 1.2U_{eq}$. All refinements were performed using the X-STEP32 crystallographic software package.[28] Structural illustrations have been drawn with ORTEP-3[29] and MERCURY.[30] Crystallographic data for compounds **1**−**12** are listed in Table 1. Selected bond distances and angles are summarized in Table 2. As expected, the highest peaks and deepest holes for these mercury complexes are slightly high, but the residual densities are close to heavy mercury atoms (with a maximum distance of 1.21 Å from Hg1 in complex **1**). For compounds **5** and **11**, which have high residual densities, the highest peaks and deepest holes are close to the Hg atoms with a distance of 0.86 and 0.79 Å for the highest peaks and 0.89 and 0.85 Å for deepest holes, respectively.

Synthesis of *N*-(3-Halophenyl)pyrazine-2-carboxamide ligands, L^{H}, $L^{3\text{-F}}$, $L^{3\text{-Cl}}$, $L^{3\text{-Br}}$, and $L^{3\text{-I}}$. These ligands were prepared by using the previously reported method.[13]

Synthesis of $[HgCl_2(L^{H})]_n$, 1. To a solution of $HgCl_2$ (0.027 g, 0.1 mmol) in 3 mL of methanol was added a solution of L^{H} (0.019 g, 0.1 mmol) in 3 mL of methanol while stirring. The mixture was heated at 40 °C for about 1 h and then filtered. Upon slow evaporation of the filtrate at room temperature, suitable yellow cystals of complex **1** for X-ray analysis were obtained after 5 days (yield 41%, mp = 153−155 °C). Anal. Calcd for $C_{11}H_9Cl_2HgN_3O$: C, 28.07; H, 1.93; N, 8.93. Found: C, 28.05; H, 1.95; N, 8.94. FT-IR (CsI pellet, cm^{-1}): 3337 (N-H str. vib.), 1666 (C═O amide str. vib.), 1606, 1540 (C-N str. and N-H bend vib.), 1434(C═C str. vib.), 1387 (C-N str. vib.), 1016, 877, 685 (O═C-N group bend vib.), 572 (O═C-N group bend vib), 439. ^{1}H NMR (CD_3OD, δ from TMS): 10.71 (s, 1H-pyrazine), 9.30 (s, amidic H), 8.93 (d, 1H-pyrazine), 8.81−8.83 (m, 1H-pyrazine), 7.89 (d, 2H-phenyl), 7.37 (t, 2H-phenyl), and 7.14 (t, 1H-phenyl).

Synthesis of $[HgCl_2(L^{3\text{-Cl}})]_n$, 2. The procedure was similar to the synthesis of **1** except that $L^{3\text{-Cl}}$ (0.023 g, 0.1 mmol) was used instead of L^{H}. Colorless crystals of **2** were formed after 5 days (yield 72%, mp = 184−186 °C). Anal. Calcd for $C_{11}H_8Cl_3HgN_3O$: C, 26.15; H, 1.60; N, 8.32. Found: C, 26.13; H, 1.58; N, 8.30. FT-IR (CsI pellet, cm^{-1}): 3356 (N-H str. vib.), 1692 (C═O amide str. vib.), 1600, 1527 (C-N str. and N-H bend vib.), 1474 (C═C str. vib.), 1420, 1394 (C-N str. vib.), 1122 (C-Cl str. vib.), 1049, 844, 777, 678 (O═C-N group bend vib.), 579 (O═C-N group bend vib), 426. ^{1}H NMR (CD_3OD, δ from TMS): 10.96 (s, 1H-pyrazine), 9.30 (s, amidic H), 8.95 (d, 1H-pyrazine), 8.82−8.84 (m, 1H-pyrazine), 8.09 (s, 1H-phenyl), 7.86 (d, 1H-phenyl), 7.40 (t, 1H-phenyl), and 7.20 (d, 1H-phenyl).

Synthesis of $[Hg_2Cl_4(L^{3\text{-Br}})_2]$, 3. The procedure was similar to the synthesis of **1** except that $L^{3\text{-Br}}$ (0.027 g, 0.1 mmol) was used instead of L^{H}. Colorless crystals of **3** were formed after 7 days (yield 69%, mp = 196−198 °C). The complex **3** is relatively stable in the solid state when stored in the mother liquor, but decomposes slowly when exposed to open air. Therefore, the diffraction data for this compound were collected at 173 K. Anal. Calcd for $C_{22}H_{16}Br_2Cl_4Hg_2N_6O_2$: C, 24.04; H, 1.47; N, 7.65. Found: C, 24.01; H, 1.45; N, 7.63. FT-IR (CsI pellet, cm^{-1}): 3350 (N-H str. vib.), 1692 (C═O amide str. vib.), 1659 (C═O amide str. vib.), 1573 (C-N str. and N-H bend vib.), 1467 (C═C str. vib.), 1394 (C-N str. vib.), 1122 (C-Br str. vib.), 857, 685 (O═C-N group bend vib.), 579 (O═C-N group bend vib), 433. ^{1}H NMR (CD_3OD, δ from TMS): 10.91 (s, 1H-pyrazine), 9.29 (s, amidic H), 8.95 (d, 1H-pyrazine), 8.81−8.84 (m, 1H-pyrazine), 8.24 (s, 1H-phenyl), 7.90 (d, 1H-phenyl), 7.56 (d, 1H-phenyl), and 7.35 (t, 1H-phenyl).

Synthesis of $[Hg_2Cl_4(L^{3\text{-I}})_2]$, 4. The procedure was similar to the synthesis of **1** except that $L^{3\text{-I}}$ (0.032 g, 0.1 mmol) was used instead of L^{H}. Light yellow crystals of **4** were formed after 2 weeks (yield 55%, mp = 200−202 °C). Anal. Calcd for $C_{22}H_{16}Cl_4Hg_2I_2N_6O_2$: C, 22.15; H, 1.35; N, 7.04. Found: C, 22.14; H, 1.35; N, 7.04. FT-IR (CsI pellet, cm^{-1}): 3337 (N-H str. vib.), 1692 (C═O amide str. vib.), 1675 (C═O amide str. vib.), 1573 (C-N str. and N-H bend vib.), 1533, 1467 (C═C str. vib.), 1394 (C−N str. vib.), 1116 (C-I str. vib), 1016, 850, 685 (O═C-N group bend vib.), 585 (O═C-N group bend vib), 435. ^{1}H NMR (CD_3OD, δ from TMS): 10.83 (s, 1H-pyrazine), 9.28 (s, amidic H), 8.93 (d, 1H-pyrazine), 8.79−8.82 (m, 1H-pyrazine), 8.38 (s, 1H-phenyl), 7.90 (d, 1H-phenyl), 7.50 (d, 1H-phenyl), and 7.17 (t, 1H-phenyl).

Synthesis of $[Hg_2Br_4(L^{H})_2]$, 5. The procedure was similar to the synthesis of **1** except that $HgBr_2$ (0.036 g, 0.1 mmol) was used instead of $HgCl_2$. Colorless crystals of **5** were formed after 5 weeks (yield 69%, mp = 146−148 °C). Anal. Calcd for $C_{22}H_{18}Br_4Hg_2N_6O_2$: C, 23.61; H, 1.62; N, 7.51. Found: C, 23.60; H, 1.60; N, 7.50. FT-IR (CsI pellet, cm^{-1}):

dx.doi.org/10.1021/ic3021113 | *Inorg. Chem.* 2013, 52, 2891−2905

3343 (N-H str. vib.), 1672 (C═O amide str. vib.), 1546 (C-N str. and N-H bend vib.), 1447 (C═C str. vib.), 1401 (C-N str. vib.), 1016, 744, 685 (O═C-N group bend vib.), 579 (O═C-N group bend vib), 453. ^{1}H NMR (CD_3OD, δ from TMS): 10.72 (s, 1H-pyrazine), 9.29 (s, amidic H), 8.91 (d, 1H-pyrazine), 8.79−8.83 (m, 1H-pyrazine), 7.88 (d, 2H-phenyl), 7.36 (t, 2H-phenyl), and 7.16 (t, 1H-phenyl).

Synthesis of [$HgBr_2(L^{3\text{-}F})$], 6. The procedure was similar to the synthesis of **5** except that $L^{3\text{-}F}$ (0.021 g, 0.1 mmol) was used instead of L^H. Colorless crystals of **6** were formed after 7 days (yield 48%, mp = 156−158 °C). Anal. Calcd for $C_{11}H_8Br_2FHgN_3O$: C, 22.87; H, 1.40; N, 7.27. Found: C, 22.87; H, 1.40; N, 7.29. FT-IR (CsI pellet, cm^{-1}): 3339 (N-H str. vib.), 1694 (C═O amide str. vib.), 1617, 1544 (C-N str. and N-H bend vib.), 1445 (C═C str. vib.), 1407 (C-N str. vib.), 1272, 1146 (C-F str. vib), 860, 680 (O═C-N group bend vib.), 580 (O═C-N group bend vib), 459. ^{1}H NMR (CD_3OD, δ from TMS): 10.98 (s, 1H-pyrazine), 9.31 (s, amidic H), 8.95 (d, 1H-pyrazine), 8.81−8.83 (m, 1H-pyrazine), 7.85 (d, 1H-phenyl), 7.75 (d, 1H-phenyl), 7.41 (dd, 1H-phenyl), and 6.97 (t, 1H-phenyl).

Synthesis of [$HgBr_2(L^{3\text{-}Cl})$], 7. The procedure was similar to the synthesis of **5** except that $L^{3\text{-}Cl}$ (0.023 g, 0.1 mmol) was used instead of L^H. Colorless crystals of **7** were formed after 5 days (yield 45%, mp = 185−187 °C). Anal. Calcd for $C_{11}H_8Br_2ClHgN_3O$: C, 22.24; H, 1.36; N, 7.07. Found: C, 22.23; H, 1.36; N, 7.06. FT-IR (CsI pellet, cm^{-1}): 3350 (N-H str. vib.), 1686 (C═O amide str. vib.), 1586, 1533 (C-N str. and N-H bend vib.), 1440 (C═C str. vib.), 1414 (C-N str. vib.), 1129 (C-Cl str. vib.), 1049, 857, 784, 685 (O═C-N group bend vib.), 572 (O═C-N group bend vib), 453. ^{1}H NMR (CD_3OD, δ from TMS): 10.95 (s, 1H-pyrazine), 9.31 (s, amidic H), 8.95 (d, 1H-pyrazine), 8.81−8.83 (m, 1H-pyrazine), 8.09 (s, 1H-phenyl), 7.85 (d, 1H-phenyl), 7.40 (t, 1H-phenyl), and 7.20 (d, 1H-phenyl).

Synthesis of [$HgBr_2(L^{3\text{-}Br})$], 8. The procedure was similar to the synthesis of **5** except that $L^{3\text{-}Br}$ (0.027 g, 0.1 mmol) was used instead of L^H. Colorless crystals of **8** were formed after 2 weeks (yield 63%, mp = 190−192 °C). Anal. Calcd for $C_{11}H_8Br_3HgN_3O$: C, 20.69; H, 1.26; N, 6.58. Found: C, 20.69; H, 1.26; N, 6.58. FT-IR (CsI pellet, cm^{-1}): 3350 (N-H str. vib.), 1699 (C═O amide str. vib.), 1573, 1540 (C-N str. and N-H bend vib.), 1474 (C═C str. vib.), 1410 (C-N str. vib.), 1129 (C-Br str. vib), 850, 771, 681 (O═C-N group bend vib.), 579 (O═C-N group bend vib), 433. ^{1}H NMR (CD_3OD, δ from TMS): 10.96 (s, 1H-pyrazine), 9.30 (s, amidic H), 8.94 (d, 1H-pyrazine), 8.80−8.83 (m, 1H-pyrazine), 8.23 (s, 1H-phenyl), 7.89 (d, 1H-phenyl), 7.56 (d, 1H-phenyl), and 7.34 (t, 1H-phenyl).

Synthesis of [$HgBr_2(L^{3\text{-}I})$], 9. The procedure was similar to the synthesis of **5** except that $L^{3\text{-}I}$ (0.032 g, 0.1 mmol) was used instead of L^H. Colorless crystals of **9** were formed after 5 days (yield 61%, mp = 191−193 °C). Anal. Calcd for $C_{11}H_8Br_2HgIN_3O$: C, 19.27; H, 1.18; N, 6.13. Found: C, 19.27; H, 1.17; N, 6.13. FT-IR (CsI pellet, cm^{-1}): 3337 (N-H str. vib.), 1686 (C═O amide str. vib.), 1586, 1533 (C-N str. and N−H bend vib.), 1460 (C═C str. vib.), 1402 (C-N str. vib.), 1122 (C-I str. vib), 1009, 850, 784, 685 (O═C-N group bend vib.), 585 (O═C-N group bend vib), 413. ^{1}H NMR (CD_3OD, δ from TMS): 10.88 (s, 1H-pyrazine), 9.31 (s, amidic H), 8.95 (d, 1H-pyrazine), 8.79−8.83 (m, 1H-pyrazine), 8.31 (s, 1H-phenyl), 7.89 (d, 1H-phenyl), 7.51 (d, 1H-phenyl), and 7.18 (t, 1H-phenyl).

Synthesis of [$Hg_2I_4(L^H)_2$], 10. The procedure was similar to the synthesis of **1** except that HgI_2 (0.045 g, 0.1 mmol) was used instead of $HgCl_2$. Colorless crystals of **10** were formed after 4 days (yield 59%, mp = 140−142 °C). Anal. Calcd for $C_{22}H_{18}Hg_2I_4N_6O_2$: C, 20.21; H, 1.39; N, 6.43. Found: C, 20.19; H, 1.38; N, 6.42. FT-IR (CsI pellet, cm^{-1}): 3360 (N-H str. vib.), 1695 (C═O amide str. vib.), 1533 (C-N str. and N-H bend vib.), 1445 (C═C str. vib.), 1387 (C-N str. vib.), 1308, 1155, 883, 685 (O═C-N group bend vib.), 587 (O═C-N group bend vib), 433. ^{1}H NMR (CD_3OD, δ from TMS): 10.73 (s, 1H-pyrazine), 9.28 (s, amidic H), 9.28 (d, 1H-pyrazine), 8.79−8.83 (m, 1H-pyrazine), 7.87 (d, 2H-phenyl), 7.37 (t, 2H-phenyl), and 7.15 (t, 1H-phenyl).

Synthesis of [$HgI_2(L^{3\text{-}Br})$], 11. The procedure was similar to the synthesis of **10** except that $L^{3\text{-}Br}$ (0.027 g, 0.1 mmol) was used instead of L^H. Colorless crystals of **11** were formed after 2 weeks (yield 51%, mp = 200−202 °C). Anal. Calcd for $C_{11}H_8BrHgI_2N_3O$: C, 18.04; H, 1.10; N, 5.74. Found: C, 18.03; H, 1.10; N, 5.72. FT-IR (CsI pellet, cm^{-1}): 3350 (N-H str. vib.), 1692 (C═O amide str. vib.), 1540 (C-N str. and N-H bend vib.), 1474 (C═C str. vib.), 1401 (C-N str. vib.), 1175, 1122 (C-Br str. vib.), 1056, 850, 671 (O═C-N group bend vib.), 585 (O═C-N group bend vib), 433. ^{1}H NMR (CD_3OD, δ from TMS): 10.93 (s, 1H-pyrazine), 9.29 (s, amidic H), 8.95 (d, 1H-pyrazine), 8.79−8.83 (m, 1H-pyrazine), 8.23 (s, 1H-phenyl), 7.88 (d, 1H-phenyl), 7.56 (d, 1H-phenyl), and 7.33 (t, 1H-phenyl).

Synthesis of [$HgI_2(L^{3\text{-}I})$], 12. The procedure was similar to the synthesis of **10** except that $L^{3\text{-}I}$ (0.032 g, 0.1 mmol) was used instead of L^H. Colorless crystals of **11** were formed after 2 weeks (yield 42%, mp = 207−209 °C). Anal. Calcd for $C_{11}H_8HgI_3N_3O$: C, 16.95; H, 1.03; N, 5.39. Found: C, 16.95; H, 1.02; N, 5.37. FT-IR (CsI pellet, cm^{-1}): 3343 (N-H str. vib.), 1692 (C═O amide str. vib.), 1540 (C-N str. and N-H bend vib.), 1467 (C═C str. vib.), 1381 (C-N str. vib.), 1122 (C-I str. vib.), 850, 777, 671 (O═C-N group bend vib.), 585 (O═C-N group bend vib), 459. ^{1}H NMR (CD_3OD, δ from TMS): 10.86 (s, 1H-pyrazine), 9.29 (s, amidic H), 8.94 (d, 1H-pyrazine), 8.79−8.82 (m, 1H-pyrazine), 8.32 (s, 1H-phenyl), 7.90 (d, 1H-phenyl), 7.50 (d, 1H-phenyl), and 7.17 (t, 1H-phenyl).

Computational Details. DFT calculations were performed using the ORCA quantum chemistry suite.[31] The local density approximation (LDA) exchange correlation potential was used with the local density approximation of the correlation energy.[32] Gradient-corrected geometry optimizations[33] were performed by using the generalized gradient approximation.[34] Large atom basis sets TZP were used to ascribe all of the atoms. Scalar relativistic effects were taken into account by using the zeroth-order regular approximation (ZORA).[35]

Thermal Analysis (TG). TG experiments were carried out using a Rheometric Scientific (STA/1500) with a heating rate of 10 °C/min in the range of 25−500 °C, under an air atmosphere. The measurements were carried out using around 10 mg of a powdered sample sealed in aluminum pans with a mechanical crimp.

■ ASSOCIATED CONTENT

Ⓢ Supporting Information

TG curves for compounds **2**, **3**, **4**, **7**, **8**, **9**, **11**, and **12**; hydrogen bond geometries, and X-ray crystallographic files in CIF format for structural determination of **1** (CCDC No. 901972), **2** (CCDC No. 901975), **3** (CCDC No. 901970), **4** (CCDC No. 901976), **5** (CCDC No. 901971), **6** (CCDC No. 901981), **7** (CCDC No. 901978), **8** (CCDC No. 901973), **9** (CCDC No. 901974), **10** (CCDC No. 901980), **11** (CCDC No. 901979), and **12** (CCDC No. 901977). This material is available free of charge *via* the Internet at http://pubs.acs.org.

■ AUTHOR INFORMATION

Corresponding Author

*Phone: +98 21 29903105. Fax: +98 21 22431661. E-mail: h-khavasi@sbu.ac.ir.

Notes

The authors declare no competing financial interest.

■ ACKNOWLEDGMENTS

We would like to thank the Graduate Study Councils of Shahid Beheshti University, General Campus, for financial support and Prof. Richard J. Staples from the Department of Chemistry, Michigan State University, for data collection on some of single crystals studied here.

■ REFERENCES

(1) (a) Ali, A.; Hundal, G.; Gupta, R. *Cryst. Growth Des.* **2012**, *12*, 1308−1319. (b) Duong, A.; Maris, T.; Wuest, J. D. *Inorg. Chem.* **2011**, *50*, 5605−5618. (c) Natale, D.; Mareque-Rivas, J. C. *Chem. Commun.* **2008**, 425−437. (d) Desiraju, G. R. *J. Chem. Soc., Dalton Trans.* **2000**, 3745−3751. (e) Nishio, M. *CrystEngComm* **2004**, *6*, 130−158. (f) Brammer, L. *Dalton Trans.* **2003**, 3145−3157.

(2) (a) Janssen, F. F. B. J.; Gelder, R. G.; Rowan, A. E. *Cryst. Growth Des.* **2011**, *11*, 4326−4333. (b) Field, J. S.; Munro, O. Q.; Waldron, B. P. *Dalton Trans.* **2012**, *41*, 5486−5496. (c) Tiekink, E. R. T.; Zukerman-Schpector, J. *CrystEngComm* **2009**, *11*, 1176−1186. (d) He, L.; Ma, D.; Duan, L.; Wei, Y.; Qiao, J.; Zhang, D.; Dong, G.; Wang, L.; Qiu, Y. *Inorg. Chem.* **2012**, *51*, 4502−4510. (e) Semeniuc, R. F.; Reamer, T. J.; Smith, M. D. *New J. Chem.* **2010**, *34*, 439−452. (f) Hay, B. P.; Bryantsev, V. S. *Chem. Commun.* **2008**, 2417−2428. (g) Mooibroek, T. J.; Gamez, P.; Reedijk, J. *CrystEngComm* **2008**, *10*, 1501−1515. (h) Schottel, B. L.; Chifotides, H. T.; Dunbar, K. R. *Chem. Soc. Rev.* **2008**, *37*, 68−83.

(3) Metrangolo, P.; Neukirch, H.; Pilati, T.; Resnati, G. . *Acc. Chem. Res.* **2005**, *38*, 386−395.

(4) (a) Desiraju, G. R.; Parthasarathy, R. *J. Am. Chem. Soc.* **1989**, *111*, 8725−8727. (b) Jagarlapudi, A. R.; Sarma, P.; Desiraju, G. R. *Acc. Chem. Res.* **1986**, *19*, 222−228. (c) Awwadi, F. F.; Willett, R. D.; Twamley, B.; Schneider, R.; Landee, C. *Inorg. Chem.* **2008**, *47*, 9327−9332. (d) Awwadi, F. F.; Willett, R. D.; Twamley, B. *Cryst. Growth Des.* **2007**, *7*, 624−632. (e) Brammer, L.; Espallargas, G. M.; Adams, H. *CrystEngComm* **2003**, *5*, 343−345. (f) Zordan, F.; Brammer, L.; Sherwood, P. *J. Am. Chem. Soc.* **2005**, *127*, 5979−5989. (g) Karpfen, A. *J. Phys. Chem. A* **2001**, *105*, 2064−2072. (h) Willett, R. D.; Awwadi, F. F.; Butcher, R.; Haddad, S. F.; Twamley, B. *Cryst. Growth Des.* **2003**, *3*, 301−311. (i) Rosokha, S. V.; Lu, J.; Rosokha, T. Y.; Kochi, J. k. *Chem. Commun.* **2007**, 3383−3385. (j) Awwadi, F. F.; Willett, R. D.; Haddad, S. F.; Twamley, B. *Cryst. Growth Des.* **2006**, *6*, 1833−1838. (k) Aakeröy, C. B.; Desper, J.; Helfrich, B. A.; Metrangolo, P.; Pilati, T.; Resnati, G.; Stevennazzi, A. *Chem. Commun.* **2007**, 4236−4238.

(5) (a) Brammer, L.; Espallargas, G. M.; Libri, S. *CrystEngComm* **2008**, *10*, 1712. (b) Mareque Rivas, J. C.; Brammer, L. *Coord. Chem. Rev.* **1999**, *183*, 43−80.

(6) Bertani, R.; Sgarbossa, P.; Venzo, A.; Lelj, F.; Amati, M.; Resnati, G.; Pilati, T.; Metrangolo, P.; Terraneo, G. *Coord. Chem. Rev.* **2010**, *254*, 677−695.

(7) Aakeröy, C. B.; Sinha, A. S.; Chopade, P. D.; Desper, J. *Dalton Trans.* **2011**, *40*, 12160−12168.

(8) Smart, P.; Espallargas, G. M.; Brammer, L. *CrystEngComm* **2008**, *10*, 1335−1344.

(9) Desiraju, G. R. *Angew. Chem., Int. Ed.* **1995**, *34*, 2311−2327.

(10) Aakeröy, C. B.; Schultheiss, N.; Desper, J.; Moore, C. *CrystEngComm* **2007**, *9*, 421−426.

(11) Derossi, S.; Brammer, L.; Hunter, C. A.; Ward, M. D. *Inorg. Chem.* **2009**, *48*, 1666−1677.

(12) (a) Khavasi, H. R.; Azizpoor Fard, M. *Cryst. Growth Des.* **2010**, *10*, 1892−1896. (b) Khavasi, H. R.; Salimi, A. R.; Eshtiagh-Hosseini, H.; Amini, M. M. *CrystEngComm* **2011**, *13*, 3710−3717. (c) Khavasi, H. R.; Mehdizadeh Barforoush, M.; Azizpoor Fard, M. *CrystEngComm* **2012**, *14*, 7236−7244.

(13) Sasan, K.; Khavasi, H. R.; Davari, M. D. *Monatsh. Chem.* **2008**, *139*, 773−780.

(14) Yang, L.; Powell, D. R.; Houser, R. P. *Dalton Trans.* **2007**, 955−964.

(15) Addison, A. W.; Rao, T. N.; Reedijk, J.; Van Rijn, J.; Verschoor, G. C. *J. Chem. Soc., Dalton Trans.* **1984**, 1349−1356.

(16) (a) Wu, J.-Y.; Hsu, H.-Y.; Chan, C.-C.; Wen, Y.-S.; Tsai, C.; Lu, K.-L. *Cryst. Growth Des.* **2009**, *9*, 258−262. (b) Popovic, Z.; Soldin, Z.; Matkovic-Calogovic, D.; Pavlovic, G.; Rajic, M.; Giester, G. *Eur. J. Inorg. Chem.* **2002**, 171−180.

(17) (a) Custelcean, R. *Chem. Soc. Rev.* **2010**, *39*, 3675−3685. (b) Mondal, R.; Basu, T.; Sadhukhan, D.; Chattopadhyay, T.; Bhunia, K. *Cryst. Growth Des.* **2009**, *9*, 1095−1105. (c) Reger, D. L.; Semeniuc, R. F.; Rassolov, V.; Smith, M. D. *Inorg. Chem.* **2004**, *43*, 537−554. (d) Schultheiss, N.; Powell, D. R.; Bosch, E. *Inorg. Chem.* **2003**, *42*, 8886−8890. (e) Bai, H.-Y.; Ma, J.-F.; Yang, J.; Liu, Y.-Y.; Wu, H.; Ma, J.-C. *Cryst. Growth Des.* **2010**, *10*, 995−1016. (f) Shatruk, M.; Chouai, A.; Dunbar, K. R. *Dalton Trans.* **2006**, 2184−2191. (g) Zhang, X.; Zhou, X.-P.; Li, D. *Cryst. Growth Des.* **2006**, *6*, 1440−1444. (h) Ni, J.; Wei, K.-J.; Liu, Y.; Huang, X.-C.; Li, D. *Cryst. Growth Des.* **2010**, *10*, 3964−3976. (i) Zhang, G.; Yang, G.; Ma, J. S. *Cryst. Growth Des.* **2006**, *6*, 1897−1902. (j) Díaz, P.; Benet-Buchholz, J.; Vilar, R.; White, A. J. P. *Inorg. Chem.* **2006**, *45*, 1617−1626. (k) Farnum, G. A.; LaDuca, R. L. *Cryst. Growth Des.* **2010**, *10*, 1897−1903. (l) Seward, C.; Chan, J.; Song, D.; Wang, S. *Inorg. Chem.* **2003**, *42*, 1112−1120. (m) Dobrzańska, L. *CrystEngComm* **2011**, *13*, 2303−2309.

(18) Notash, B.; Safari, N.; Khavasi, H. R. *Inorg. Chem.* **2010**, *49*, 11415−11420.

(19) (a) Hu, C.; Li, Q.; Englert, U. *CrystEngComm* **2003**, *5*, 519−529. (b) Lee, S. Y.; Park, S.; Kim, H. J.; Jung, J. H.; Lee, S. S. *Inorg. Chem.* **2008**, *47*, 1913−1915. (c) Wang, X.-F.; Lv, Y.; Okamura, T.-A.; Kawaguchi, H.; Wu, G.; Sun, W.-Y.; Ueyama, N. *Cryst. Growth Des.* **2007**, *7*, 1125−1133. (d) Zhou, H.-P.; Gan, X.-P.; Li, X.-L.; Liu, Z.-D.; Geng, W.-Q.; Zhou, F.-X.; Ke, W.-Z.; Wang, P.; Kong, L.; Hao, F.-Y.; Wu, J.-Y.; Tian, Y.-P. *Cryst. Growth Des.* **2010**, *10*, 1767−1776.

(20) *Cambridge Structural Database*, version 5.33; CCDC: Cambridge, U.K., November 2011.

(21) Bondi, A. *J. Phys. Chem.* **1964**, *68*, 441−451.

(22) (a) Metrangolo, G.; Resnati, G. *Halogen Bonding: Fundamentals and Applications*; Springer: Berlin, 2008. (b) Metrangolo, P.; Meyer, F.; Pilati, T.; Resnati, G.; Terraneo, G. *Angew. Chem., Int. Ed.* **2008**, *47*, 6114−6121. (c) Formiguè, M.; Batail, P. *Chem. Rev.* **2004**, *104*, 5379−5418. (d) Politzer, P.; Murray, J. S.; Clark, T. *Phys. Chem. Chem. Phys.* **2010**, *12*, 7748−7757. (e) Legon, A. C. *Angew. Chem., Int. Ed.* **1999**, *38*, 2686−2714. (f) Metrangolo, P.; Neukirch, H.; Pilati, T.; Resnati, G. *Acc. Chem. Res.* **2005**, *38*, 386−395. (g) Cavallo, G.; Metrangolo, P.; Pilati, T.; Resnati, G.; Sansoteraa, M.; Terraneo, G. *Chem. Soc. Rev.* **2010**, *39*, 3772−3783. (h) Metrangolo, P.; Neukirch, H.; Pilati, T.; Resnati, G. *Acc. Chem. Res.* **2005**, *38*, 386−395. (i) Metrangolo, P.; Resnati, G. *Science* **2008**, *321*, 918−919. (j) Murray, J. S.; Riley, K. E.; Politzer, P.; Clark, T. *Aust. J. Chem.* **2010**, *63*, 1598−1607.

(23) Ananthavel, S. P.; Manoharan, M. *Chem. Phys.* **2001**, *269*, 49−57.

(24) Rissanen, K. *CrystEngComm* **2008**, *10*, 1107−1113.

(25) (a) *COSMO V1.58: Software for the CCD Detector Systems for Determining DataCollection Parameters*; Bruker Analytical X-ray Systems: Madison, WI, 2008. (b) *APEX2 V2008.5-0: Software for the CCD Detector System*; Bruker Analytical X-ray Systems: Madison, WI, 2008. (c) *SAINT V 7.34: Software for the Integration of CCD Detector System*; Bruker Analytical X-ray Systems: Madison, WI, 2008. (d) SADABS V2.008/2, program for absorption corrections using Bruker-AXS CCD based on the method of Robert Blessing. Blessing, R. H. *Acta Crystallogr.* **1995**, *A51*, 33−38.

(26) (a) *X-AREA: Program for the Acquisition and Analysis of Data*, vesion 1.30; Stoe & Cie GmbH: Darmstadt, Germany, 2005. (b) *X-RED: Program for Data Reduction and Absorption Correction*, version 1.28b; Stoe & Cie GmbH: Darmstadt, Germany, 2005. (c) *X-SHAPE: Program for Crystal Optimization for Numerical Absorption Correction*, vesion 2.05; Stoe & Cie GmbH: Darmstadt, Germany, 2004.

(27) Sheldrick, G. M. *SHELX97: Program for Crystal Structure Solution and Refinement*; University of Göttingen: Göttingen, Germany, 1997.

(28) *X-STEP32: Crystallographic Package*, version 1.07b; Stoe & Cie GmbH: Darmstadt, Germany, 2000.

(29) Farrugia, L. J. *J. Appl. Crystallogr.* **2012**, *45*, 849−854.

(30) *Mercury 2.3*, supplied with cambridge structural database; CCDC: Cambridge, U.K., 2003−2004.

(31) Neese, F.; Becker, U.; Ganyushin, D.; Liakos, D. G.; Kossmann, S.; Petrenko, T.; Riplinger, C.; Wennmohs, F. *ORCA, 2.7.0*; University of Bonn: Bonn, Germany, 2009.

(32) Vosko, S. H.; Wilk, L.; Nusair, M. *Can. J. Phys* **1980**, *58*, 1200−1211.

(33) (a) Versluis, L.; Ziegler, T. *J. Chem. Phys.* **1988**, *88*, 322−328. (b) Fan, L.; Ziegler, T. *J. Chem. Phys.* **1991**, *95*, 7401−7405.

(34) Perdew, J. P.; Chevary, J. A.; Vosko, S. H.; Jackson, K. A.; Pederson, M. R.; Singh, D. J.; Fiolhais, C. *Phys. Rev.* **1992**, *46*, 6671−6687.

(35) (a) van Lenthe, E.; Baerends, E. J.; Snijders, J. G. *J. Chem. Phys.* **1993**, *99*, 4597−4610. (b) van Lenthe, E.; Baerends, E. J.; Snijders, J. G. *J. Chem. Phys.* **1994**, *101*, 9783−9792. (c) van Lenthe, E.; van Leeuwen, R.; Baerends, E. J.; Snijders, J. G. *Int. J. Quantum Chem.* **1996**, *57*, 281−293.